ESC European Society of Cardiology

Cardiovascular Research (2022) **118**, 1917–1931
https://doi.org/10.1093/cvr/cvab245

Natriuretic peptide receptor B maintains heart rate and sinoatrial node function via cyclic GMP-mediated signalling

Tristan W. Dorey[1], Martin Mackasey[1], Hailey J. Jansen [1], Megan D. McRae[1], Loryn J. Bohne[1], Yingjie Liu[1], Darrell D. Belke[1], Logan Atkinson[2], and Robert A. Rose [1]*

[1]Department of Cardiac Sciences, Department of Physiology and Pharmacology, Libin Cardiovascular Institute, Cumming School of Medicine, University of Calgary, GAC66, Health Research Innovation Centre, 3280 Hospital Drive N.W., Calgary, AB T2N 4Z6, Canada and [2]Department of Physiology and Biophysics, Faculty of Medicine, Dalhousie University, Halifax, NS, Canada

Received 22 January 2021; editorial decision 8 July 2021; accepted 16 July 2021; online publish-ahead-of-print 17 July 2021

Aims Heart rate (HR) is a critical indicator of cardiac performance that is determined by sinoatrial node (SAN) function and regulation. Natriuretic peptides, including C-type NP (CNP), have been shown to modulate ion channel function in the SAN when applied exogenously. CNP is the only NP that acts as a ligand for natriuretic peptide receptor-B (NPR-B). Despite these properties, the ability of CNP and NPR-B to regulate HR and intrinsic SAN automaticity *in vivo*, and the mechanisms by which it does so, are incompletely understood. Thus, the objective of this study was to determine the role of NPR-B signalling in regulating HR and SAN function.

Methods and results We have used NPR-B deficient mice (NPR-B$^{+/-}$) to study HR regulation and SAN function using telemetry in conscious mice, intracardiac electrophysiology in anaesthetized mice, high-resolution optical mapping in isolated SAN preparations, patch-clamping in isolated SAN myocytes, and molecular biology in isolated SAN tissue. These studies demonstrate that NPR-B$^{+/-}$ mice exhibit slow HR, increased corrected SAN recovery time, and slowed SAN conduction. Spontaneous AP firing frequency in isolated SAN myocytes was impaired in NPR-B$^{+/-}$ mice due to reductions in the hyperpolarization activated current (I_f) and L-type Ca^{2+} current ($I_{Ca,L}$). I_f and $I_{Ca,L}$ were reduced due to lower cGMP levels and increased hydrolysis of cAMP by phosphodiesterase 3 (PDE3) in the SAN. Inhibiting PDE3 or restoring cGMP signalling via application of 8-Br-cGMP abolished the reductions in cAMP, AP firing, I_f, and $I_{Ca,L}$, and normalized SAN conduction, in the SAN in NPR-B$^{+/-}$ mice. NPR-B$^{+/-}$ mice did not exhibit changes in SAN fibrosis and showed no evidence of cardiac hypertrophy or changes in ventricular function.

Conclusions NPR-B plays an essential physiological role in maintaining normal HR and SAN function by modulating ion channel function in SAN myocytes via a cGMP/PDE3/cAMP signalling mechanism.

*Corresponding author. Tel: 403 210 3922; fax: 403 270 0313, E-mail: robert.rose@ucalgary.ca

Graphical Abstract

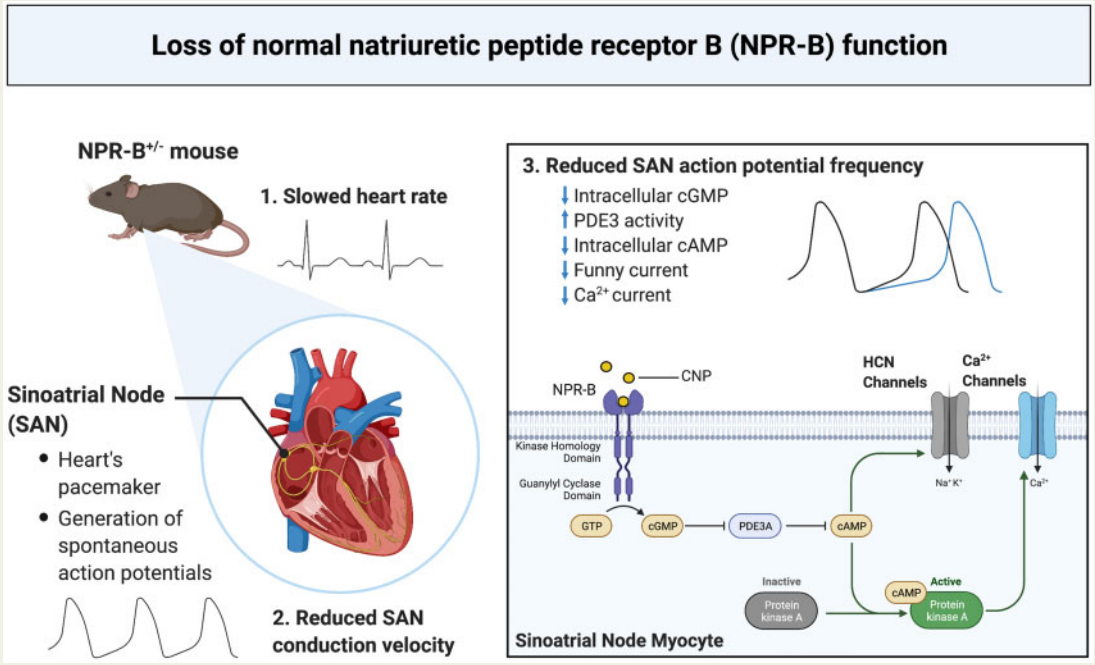

Keywords Natriuretic peptides • Natriuretic peptide receptors • Sinoatrial node • Heart rate • Phosphodiesterase

1. Introduction

Heart rate (HR) is determined by a specialized group of cells located in the sinoatrial node (SAN) within the right atrium of the heart. The SAN generates spontaneous action potentials (APs), the frequency of which determines intrinsic heart rate (HR) *in vivo*.[1] Spontaneous APs in SAN myocytes occur due to the presence of a diastolic depolarization (DD) between successive APs. The hyperpolarization-activated current (I_f, carried by HCN channels) and the L-type Ca^{2+} current ($I_{Ca,L}$, carried by $Ca_V1.2$ and $Ca_V1.3$ channels) play critical roles in determining the slope of the DD and the frequency of spontaneous AP firing in SAN myocytes.[1,2] Conduction within the SAN and from the SAN to the atria is also affected by Na^+ current (I_{Na}) and gap junctions formed by connexins (Cx).[3–5] HR and SAN function can be modified by both neural and humoral factors in order to regulate cardiac performance.[6] For example, AP firing and ion channel function in the SAN are regulated by cyclic nucleotides, such as cyclic GMP (cGMP) and cyclic AMP (cAMP), enabling regulation of HR to meet physiological demands.[1,6] Cyclic nucleotide levels in cardiomyocytes are critically regulated by phosphodiesterases (PDEs), which are the primary enzymes responsible for the degradation of cGMP and cAMP.[7]

Natriuretic peptides (NPs) are a family of cardioprotective hormones composed of atrial (ANP), B-type (BNP), and C-type (CNP) NPs that play important roles in maintaining cardiovascular homeostasis.[8–10] NPs bind to three distinct membrane receptors (NPRs) called NPR-A, NPR-B, and NPR-C, all of which are expressed in the SAN.[8,11] CNP is the lone agonist for NPR-B, which is a particulate guanylyl cyclase (GC) linked receptor that increases intracellular cGMP concentration upon receptor activation.[8]

NPs are produced in the atrial myocardium where they can be released into the circulation or exert local effects within the heart.[8,10] CNP is present at very low levels in the circulation suggesting it mainly acts through local paracrine mechanisms.[10] Previous studies demonstrate that acute activation of NPR-B by exogenous application of CNP can potently regulate HR and SAN function.[11–14] Furthermore, alterations in the expression of NPR-B have been noted in a number of disease conditions[15–18] that are associated with reduced HR or impaired SAN function[19,20] suggesting that NPR-B may play an important role in maintaining normal SAN physiology. Nevertheless, how NPR-B contributes to the maintenance of normal intrinsic SAN automaticity *in vivo* remains incompletely understood. Accordingly, the goal of the present study was to determine how NPR-B deficiency impacts HR and SAN function using mice with a heterozygous deletion of NPR-B ($NPR\text{-}B^{+/-}$). Our findings demonstrate that NPR-B plays an essential physiological role in maintaining SAN automaticity via cGMP-mediated effects on ion channel function in SAN myocytes.

2. Methods

2.1 Mice

This study was conducted using male and female $NPR\text{-}B^{+/-}$ mice and wildtype littermate controls. All experimental procedures were ap-

proved by the University of Calgary Animal Care and Use Committee or the Dalhousie University Committee for Laboratory Animals and were in accordance with the guidelines of the Canadian Council on Animal Care and the NIH guide for the care and use of laboratory animals.

2.2 Experimental techniques

HR, heart rate variability (HRV), and SAN function were assessed in anaesthetized mice *in vivo* using intracardiac electrophysiology[21,22] or in conscious mice using telemetry.[23,24] SAN function and conduction patterns were assessed using high-resolution optical mapping in isolated SAN preparations.[12,21] Spontaneous AP firing patterns and ionic currents (I_f, $I_{Ca,L}$, I_{Na}) were investigated using patch-clamping in isolated SAN myocytes.[21,22] Cyclic nucleotide (cAMP and cGMP) levels and PDE activity were assessed using commercially available kits. SAN mRNA expression and protein levels were investigated using qPCR and Western blotting.[22,25] SAN fibrosis was assessed using histology and immunohistochemistry.[22] Cardiac structure was measured in anaesthetized mice by echocardiography.[22,26] Blood pressure was measured in conscious, restrained mice by tail-cuff plethysmography.[26,27] For surgeries and tissue isolations, mice were anaesthetized using isoflurane (2%, inhalation). Mice were euthanized by cervical dislocation under isoflurane anaesthesia. Expanded details for these experimental techniques are available in the Supplementary material online.

2.3 Statistics

All data are presented as means ± SEM. Statistical analysis was conducted using Prism version 8.3.1 (GraphPad Software). Data were analysed using Student's *t*-test, two-way analysis of variance (ANOVA) with a Holm–Sidak *post hoc* test, two-way repeated-measures ANOVA with a Holm–Sidak *post hoc* test, or a Fisher's exact test as indicated in each figure legend. Non-parametric data were analysed by Mann–Whitney *U* test where indicated. $P < 0.05$ was considered significant.

3. Results

3.1 Effects of NPR-B deficiency on HR and SAN function *in vivo*

Initially, the mRNA and protein expression of NPR-A, NPR-B, and NPR-C were measured in the SAN of wildtype and NPR-B$^{+/-}$ mice. NPR-B mRNA and protein levels were reduced by ∼50% in the SAN in NPR-B$^{+/-}$ mice (Supplementary material online, *Figure S1*). NPR-A and NPR-C mRNA expression and protein levels were unchanged in the SAN of NPR-B$^{+/-}$ mice (Supplementary material online, *Figure S1*). NPR-B mRNA and protein levels were also reduced in the atria and left ventricle in NPR-B$^{+/-}$ mice (Supplementary material online, *Figure S1*).

Next, HR was assessed in awake, freely moving wildtype and NPR-B$^{+/-}$ mice using telemetric ECG recordings. HR was reduced in NPR-B$^{+/-}$ mice (*Figure 1A,B*) as indicated by lower average HRs during the day and night phases of the diurnal cycle (*Figure 1C*). SAN dysfunction was evident in NPR-B$^{+/-}$ mice as shown by an increase in spontaneous sinus pause incidence compared to wildtype controls (*Figure 1D,E*). There was no difference in the duration of sinus pauses between genotypes (*Figure 1F*).

SAN function was assessed directly by intracardiac programmed stimulation to measure corrected SAN recovery time (cSNRT) in anaesthetized mice (*Figure 1G*). These data demonstrate that cSNRT was prolonged in NPR-B$^{+/-}$ mice compared to wildtype controls (*Figure 1H*). SAN dysfunction can affect male and female patients;[28] therefore, HR and cSNRT were also stratified by sex in wildtype and NPR-B$^{+/-}$ mice. HR was reduced and cSNRT recovery time was prolonged similarly in NPR-B$^{+/-}$ mice of both sexes (Supplementary material online, *Figure S2*); thus, male and female data were combined for subsequent analysis.

HR was also assessed as a function of activity from telemetric ECG recordings (Supplementary material online, *Figure S3*). As expected, HR was higher during high activity phases; however, HR remained reduced in NPR-B$^{+/-}$ mice during both low and high activity. There were no differences in activity levels between WT and NPR-B$^{+/-}$ mice (Supplementary material online, *Figure S3*). Maximum HR elicited by the injection of isoproterenol (ISO; 10 mg/kg) was also assessed (Supplementary material online, *Figure S3*). ISO increased HR similarly in both genotypes such that maximum HR was reduced in NPR-B$^{+/-}$ mice.

Additional measures of cardiac conduction were assessed from the surface and intracardiac ECG recordings that included His bundle signals (Supplementary material online, *Figure S4*). AV node effective refractory period was prolonged in NPR-B$^{+/-}$ mice; however, there were no differences in PR interval, AH interval, or HV interval between genotypes (Supplementary material online, *Figure S4*).

3.2 Autonomic nervous system activity in NPR-B deficient mice

NPs can regulate autonomic nervous system (ANS) function,[29] which could have an impact on resting or intrinsic HR. This was assessed by determining if NPR-B deficiency affects heart rate variability (HRV; a surrogate marker of ANS activity[30]) or the HR response to ANS blockers in conscious mice (*Figure 2*). Total HRV, as assessed by the standard deviation of R-R intervals (SDNN), was increased in NPR-B$^{+/-}$ mice compared to wildtypes during the low activity phase. High activity reduced SDNN in both groups with NPR-B$^{+/-}$ mice trending ($P = 0.11$) towards higher SDNN during the high activity phase (*Figure 2A*). It is important to recognize that HR itself, which is reduced in NPR-B$^{+/-}$ mice, has an important effect on overall HRV.[31] Accordingly, SDNN was corrected for HR by plotting SDNN from high and low activity phases in wildtype and NPR-B$^{+/-}$ mice as a function of the corresponding HR and fitting the data with an exponential equation (*Figure 2B*). Linear regression analysis of the relationship between SDNN and HR shows an R^2 value of 0.71 indicating that HR accounts for 71% of the variation in SDNN in these mice. When corrected for HR, there were no differences in SDNN (cSDNN) between wildtype and NPR-B$^{+/-}$ mice during high and low activity phases (*Figure 2C*).

Consistent with the increased SDNN in NPR-B$^{+/-}$ mice, power spectral density plots (baseline conditions) demonstrate that total power, low-frequency (LF) power, and high-frequency (HF) power were all increased in NPR-B$^{+/-}$ mice (*Figure 2D–G*). Similar to cSDNN, when LF power and HF power were normalized to total power, no differences in frequency domain metrics of HRV between wildtype and NPR-B$^{+/-}$ mice were observed (*Figure 2H*).

HRV was also assessed using Poincaré plots measured at baseline and after autonomic nervous system (ANS) blockade following combined injection of atropine (10 mg/kg) and propranolol (10 mg/kg) (Supplementary material online, *Figure S5*). Standard deviations from these Poincaré plots (i.e. SD1 and SD2) were larger in NPR-B$^{+/-}$ mice at baseline and after ANS blockade (Supplementary material online, *Figure S5*).

To further investigate ANS regulation of HR, wildtype and NPR-B$^{+/-}$ mice were injected with atropine (10 mg/kg) and propranolol (10 mg/kg)

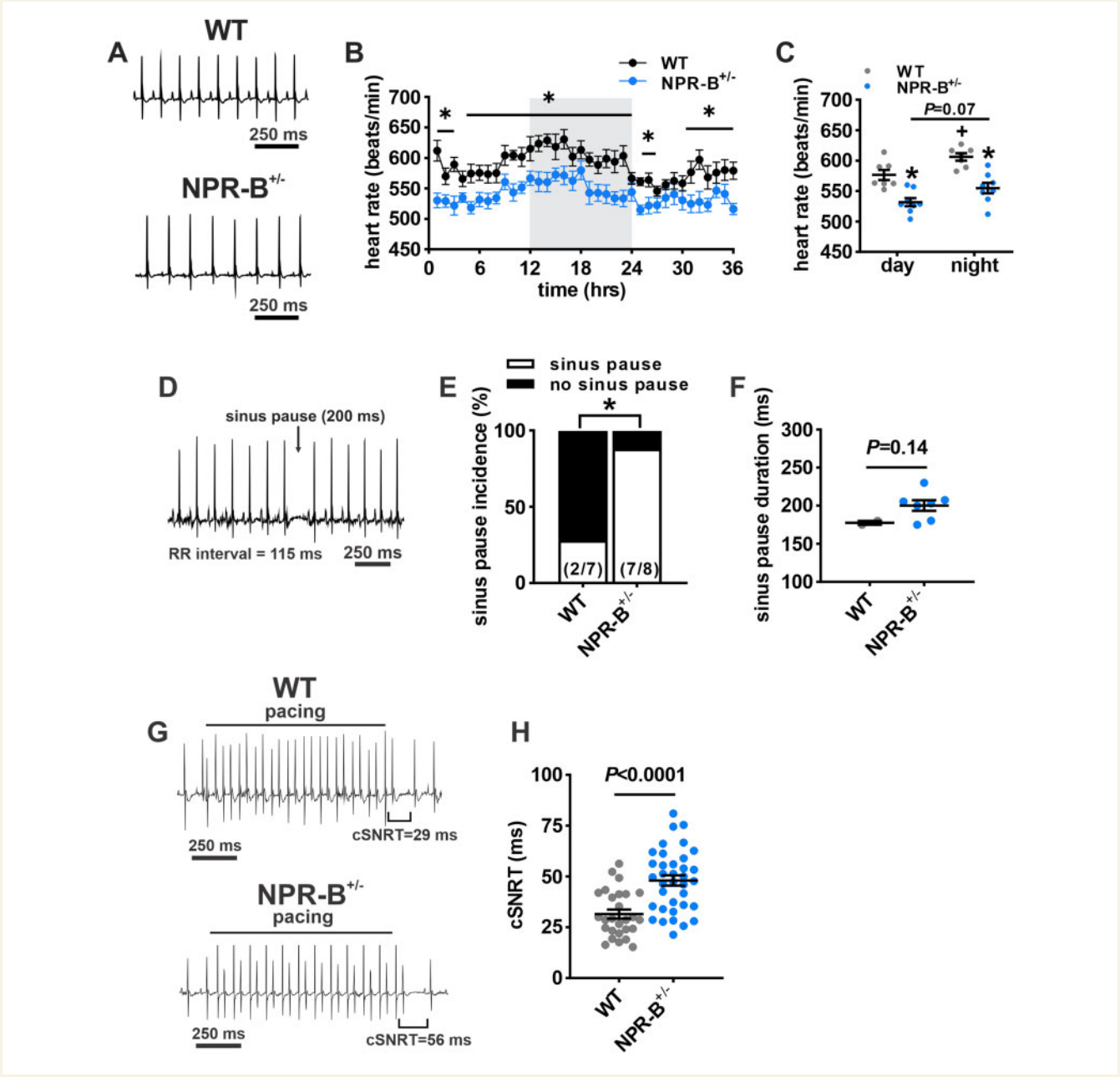

Figure 1 Heart rate and SAN function in NPR-B$^{+/-}$ mice. (*A*) Representative telemetric ECG recordings from awake and freely moving wildtype (WT) and NPR-B$^{+/-}$ mice during daytime low activity phase. (*B*) Heart rate (HR) fluctuations in WT ($n = 7$ mice) and NPR-B$^{+/-}$ ($n = 8$ mice) mice over a 36 h period. Grey shading indicates night-time hours (7:00 pm–7:00 am). *$P < 0.05$ vs. WT at the indicated timepoint by two-way ANOVA with Holm–Sidak *post hoc* test. (*C*) Summary of mean HR in WT and NPR-B$^{+/-}$ mice during day and night cycles. *$P < 0.05$ vs. WT within diurnal phase; $^{+}P < 0.05$ vs. day within genotype by two-way ANOVA with Holm–Sidak *post hoc* test. (*D*) Representative telemetric ECG recording from an NPR-B$^{+/-}$ mouse illustrating the occurrence and duration of sinus pauses. (*E*) Incidence of sinus pauses in WT and NPR-B$^{+/-}$ mice. Numbers in parentheses indicate the number of mice in each group that developed sinus pauses. *$P < 0.05$ vs. WT by Fisher's exact test. (*F*) Summary of sinus pause duration in the subset of WT ($n = 2$) and NPR-B$^{+/-}$ ($n = 7$) mice that exhibited sinus pauses. (*G*) Representative surface ECG recordings during intracardiac programmed stimulation in anaesthetized WT and NPR-B$^{+/-}$ mice. (*H*) Summary of cSNRT in WT ($n = 27$ mice) and NPR-B$^{+/-}$ ($n = 36$ mice) mice. $P < 0.001$ vs. WT by Student's *t*-test.

separately to assess parasympathetic and sympathetic nervous system regulation of HR (*Figure 2I*). Atropine increased HR while propranolol decreased HR in wildtype and NPR-B$^{+/-}$ mice compared to baseline. These effects were similar in both genotypes and HR remained lower in NPR-B$^{+/-}$ mice in all conditions. Following complete ANS blockade (Supplementary material online, *Figure S6*), intrinsic HR was lower in NPR-B$^{+/-}$ mice compared to wildtypes (*Figure 2J,K*). After ANS blockade NPR-B$^{+/-}$ mice showed trends for increases in SDNN and RMSSD

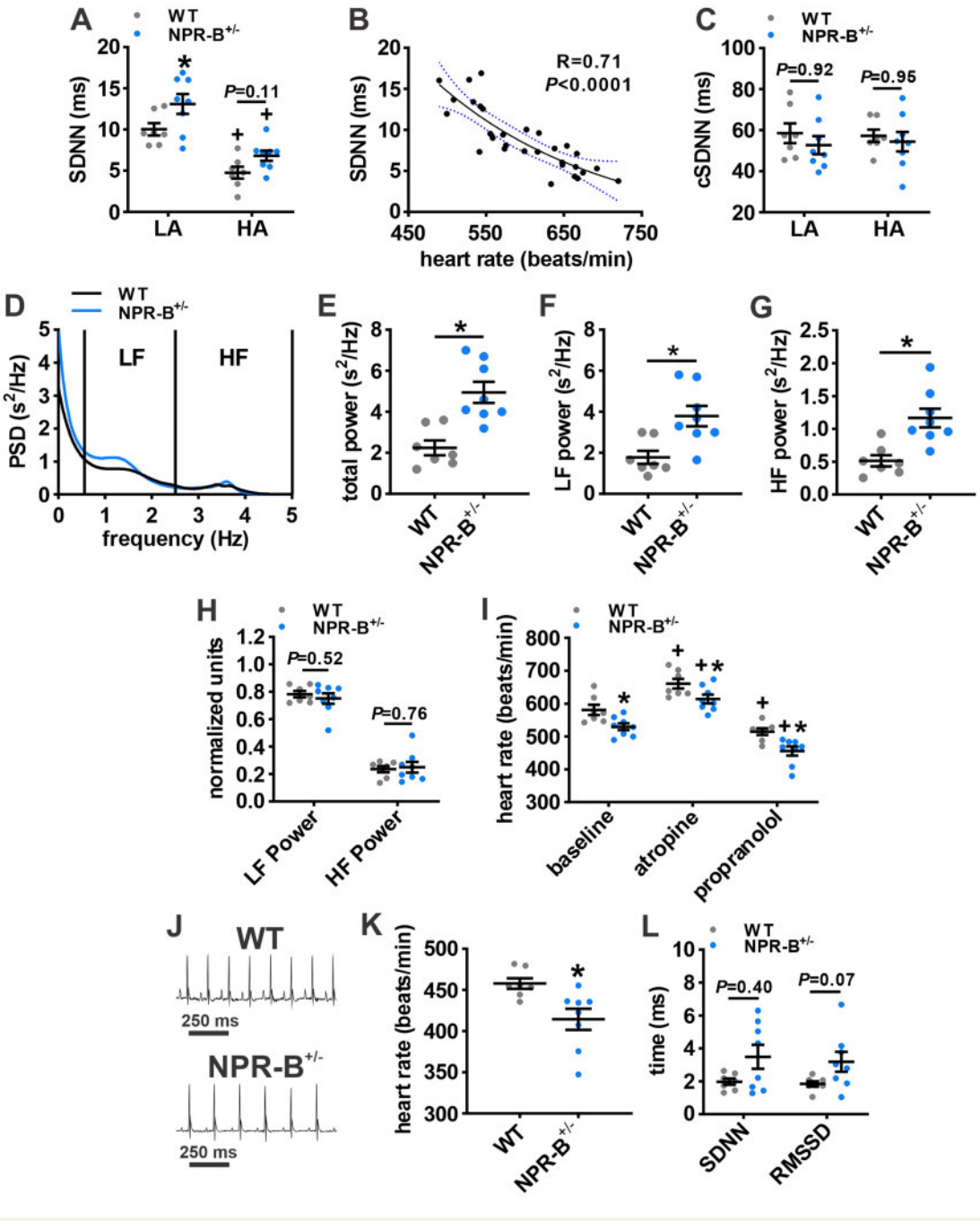

Figure 2 Autonomic regulation of HR in NPR-B$^{+/-}$ mice. (*A*) Summary of variability in RR-interval (SDNN) in WT and NPR-B$^{+/-}$ mice during low activity (LA) and high activity (HA) phases. (*B*) Plot of SDNN in WT and NPR-B$^{+/-}$ mice as a function of HR. Data were fit with an exponential function to correct for HR as detailed in the methods. Correlation coefficient obtained using Pearson's correlation. (*C*) Summary of corrected SDNN (cSDNN) in WT and NPR-B$^{+/-}$ mice. For (*A*,*C*), *$P < 0.05$ vs. WT within activity phase; $^{+}P < 0.05$ vs. low activity within genotype by two-way ANOVA with Holm–Sidak *post hoc* test. (*D*) Representative power spectral density curve for WT and NPR-B$^{+/-}$ mice showing increased power in NPR-B$^{+/-}$ mice and cut-off ranges for low-frequency (LF) and high-frequency (HF) powers. (*E–G*) Summary of total power (*E*) LF power (*F*) and HF power (*G*) in WT and NPR-B$^{+/-}$ mice. (*H*) Summary of normalized LF and HF power. For (*E–H*), *$P < 0.01$ vs. WT by Student's *t*-test. (*I*) Effects of intraperitoneal injection of atropine (10 mg/kg) or propranolol (10 mg/kg) on HR in WT and NPR-B$^{+/-}$ mice. *$P < 0.05$ vs. WT within injection condition; $^{+}P < 0.05$ vs. baseline within genotype by two-way repeated-measures ANOVA with Holm–Sidak *post hoc* test. (*J*) Telemetric ECG recordings from WT and NPR-B$^{+/-}$ mice following combined intraperitoneal injection of propranolol and atropine. (*K*,*L*), Summary data illustrating HR (*K*) and time domain measures of intrinsic HRV (SDNN, RMSSD; *L*) in NPR-B$^{+/-}$ mice following ANS blockade. *$P < 0.05$ vs. WT by Mann–Whitney Rank Sum test (SDNN) or Student's *t*-test (RMSSD). $N = 7$ WT and 8 NPR-B$^{+/-}$ mice.

(*Figure 2L*). Collectively, these data indicate that the increase in HRV observed in NPR-B$^{+/-}$ mice is due to changes in intrinsic SAN activity rather than due to changes in sympatho-vagal balance or ANS activity.

3.3 Cardiac structure and blood pressure in NPR-B deficient mice

Echocardiography was used to assess cardiac structure and function in wildtype and NPR-B$^{+/-}$ mice. M-mode imaging of the left ventricle demonstrates there were no differences in left ventricular structure or function between wildtype and NPR-B$^{+/-}$ mice (Supplementary material online, *Figure S7*). Left ventricular internal diameter, ventricular wall thickness (anterior and posterior), ejection fraction, and fractional shortening were not different between wildtype and NPR-B$^{+/-}$ mice (Supplementary material online, *Figure S7*). Furthermore, there were no differences in systolic or diastolic blood pressure between genotypes (Supplementary material online, *Figure S7*). These data demonstrate that reductions in HR and impaired SAN function in NPR-B$^{+/-}$ mice are not related to pathological changes in cardiac structure or alterations in systemic blood pressure.

To assess if the changes in HR and SAN function in NPR-B$^{+/-}$ mice were associated with structural remodelling of the pacemaker complex, SAN fibrosis was measured. Histological sections cut perpendicularly to the crista terminalis through the SAN (identified as the HCN4 positive region) demonstrate that there were no differences in SAN fibrosis between wildtype and NPR-B$^{+/-}$ mice (Supplementary material online, *Figure S8*). Similarly, there were no differences in interstitial fibrosis in the right atrium or the left ventricle in NPR-B$^{+/-}$ mice (Supplementary material online, *Figure S8*).

3.4 Effects of NPR-B deficiency on SAN electrical conduction

To directly assess electrical conduction within the SAN of wildtype and NPR-B$^{+/-}$ mice we used high-resolution optical mapping of the right atrial posterior wall adjacent to the crista terminalis, which corresponds to the anatomical position of the SAN (*Figure 3*). Activation maps in this region were used to identify the leading activation site within the SAN (*Figure 3A*). The majority of wildtype hearts had leading activation sites in the superior part of the SAN in the right atrial posterior wall as expected.[12,22,32] In contrast, NPR-B$^{+/-}$ hearts showed leading activation sites that spread across the full right atrial posterior wall from superior to inferior vena cava with more hearts demonstrating inferior leading activation sites compared to wildtype controls (*Figure 3A*).

Optical APs were recorded from the SAN in the region of the leading activation site and in the adjacent atrial myocardium (first atrial activation adjacent to the CT on the side of the right atrial free wall) (*Figure 3B*). These optical APs show that the diastolic period between successive APs is longer in NPR-B$^{+/-}$ hearts. Consistent with this, and the reduction in HR *in vivo*, atrial preparations from NPR-B$^{+/-}$ mice demonstrated lower intrinsic beating rates compared to wildtype controls (*Figure 3C*). These optical APs were also used to measure SAN to atrial conduction time (SACT) for each genotype (*Figure 3B*). SACT was longer in NPR-B$^{+/-}$ mice compared to wildtype controls (*Figure 3D*). Finally, local conduction velocity (CV) in the right atrial posterior wall (i.e. SAN region) was slower in NPR-B$^{+/-}$ mice (*Figure 3E*) which is also evident by a leftward shift in the right atrial posterior wall CV histogram from NPR-B$^{+/-}$ mice (*Figure 3F*). There were no differences in optical AP duration at 50% repolarization (APD_{50}) in the SAN region in NPR-B$^{+/-}$ mice (*Figure 3G*).

3.5 NPR-B deficiency impairs SAN myocyte electrophysiology

To further investigate the basis for SAN dysfunction in NPR-B deficient mice spontaneous APs were recorded in isolated SAN myocytes from wildtype and NPR-B$^{+/-}$ mice (*Figure 4*; Supplementary material online, *Table S1*). Consistent with the reductions in *in vivo* and *in situ* beating rates, isolated SAN myocytes from NPR-B$^{+/-}$ mice demonstrated reduced AP firing frequency (*Figure 4A,B*) and diastolic depolarization (DD) slope (*Figure 4C*) compared to wildtype controls. These differences were similar for SAN myocytes isolated from male and female wildtype and NPR-B$^{+/-}$ mice, further supporting that these findings are independent of sex (Supplementary material online, *Figure S9*). Other measurements of SAN AP morphology were not different between genotypes (Supplementary material online, *Table S1*).

The ionic basis for these alterations in SAN AP morphology was investigated next. I_f and $I_{Ca,L}$ are important contributors to DD slope and can be activated acutely by exogenous applications of NPs.[11] IV curve analysis demonstrates that I_f density was reduced in NPR-B$^{+/-}$ mice (*Figure 4D,E*). Analysis of I_f activation kinetics demonstrates that the reduction in I_f density in NPR-B$^{+/-}$ mice was associated with a leftward shift (*Figure 4F,G*) in the voltage for 50% channel activation ($V_{1/2act}$). The slope factor (k) for the I_f activation curves was not different between genotypes (Supplementary material online, *Table S2*). The time constants for I_f activation were prolonged in NPR-B$^{+/-}$ SAN myocytes (*Figure 4H*). There were no differences in expression of mRNAs for *Hcn1*, *Hcn2*, or *Hcn4* in the SAN in NPR-B$^{+/-}$ mice (Supplementary material online, *Figure S10*). Similarly, the protein levels for HCN1, HCN2, and HCN4 were not different in NPR-B$^{+/-}$ mice (Supplementary material online, *Figure S10*).

$I_{Ca,L}$ density was also reduced in SAN myocytes isolated from NPR-B$^{+/-}$ mice (*Figure 4I,J*). The reduction in $I_{Ca,L}$ occurred in association with a rightward shift in $V_{1/2(act)}$ (*Figure 4K,L*) and a reduction in maximum $I_{Ca,L}$ conductance (G_{max}; Supplementary material online, *Table S2*). There were no differences in expression of Ca^{2+} channel mRNAs (*Cacna1a* or *Cacna1d*) or $Ca_V1.2$ and $Ca_V1.3$ proteins in the SAN in NPR-B$^{+/-}$ mice (Supplementary material online, *Figure S11*).

Sodium channels have been shown to affect SAN conduction;[4] however, there were no differences in I_{Na} amplitude (Supplementary material online, *Figure S12*) or I_{Na} steady-state activation (Supplementary material online, *Figure S12*) in SAN myocytes in NPR-B$^{+/-}$ mice. Expression of *Scn5a* mRNA (encodes $Na_V1.5$ channels) was also not different in the SAN in NPR-B$^{+/-}$ mice (Supplementary material online, *Figure S12*). Finally, there were no differences in expression of *Gja5* (encodes Cx40), *Gja1* (encodes Cx43), or *Gjc1* (encodes Cx45) in the SAN in NPR-B$^{+/-}$ mice (Supplementary material online, *Figure S13*).

3.6 Cyclic nucleotide signalling in NPR-B deficient mice

Reductions in I_f and $I_{Ca,L}$ with corresponding changes in $V_{1/2(act)}$ suggests that these currents are reduced due to alterations in the biophysical modulation of these channels by cyclic nucleotides. Accordingly, we next assessed whether the reductions in AP firing in NPR-B$^{+/-}$ mice were due to alterations in SAN cyclic nucleotide handling. NPR-B is a GC-linked receptor which increases intracellular cGMP upon CNP binding.[8] Whole atrial tissue lysates from NPR-B$^{+/-}$ mice had lower levels of cGMP compared to wildtype mice (*Figure 5A*). cGMP potently inhibits PDE3 activity[7] and PDE3 plays a critical role in regulating basal SAN function by hydrolyzing cAMP;[33,34] therefore, the PDE3 inhibitor milrinone (10 μM) was used to determine the fraction of total SAN PDE activity

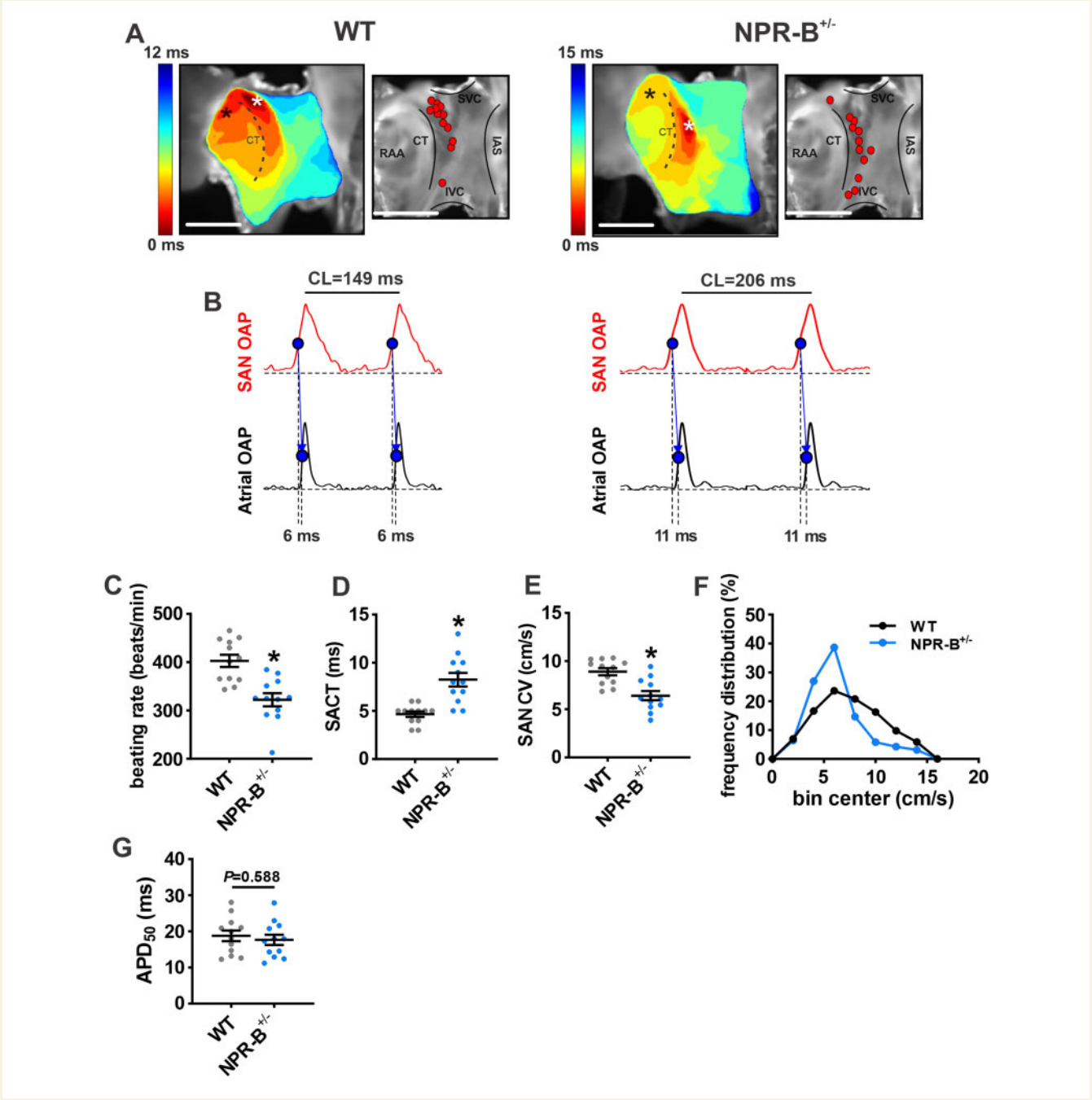

Figure 3 Assessment of electrical conduction in the SAN in NPR-B$^{+/-}$ mice. (*A*) Representative activation maps (left) and maps showing location of leading activation sites (right) for WT and NPR-B$^{+/-}$ mice. Red dots represent leading activation sites for different WT and NPR-B$^{+/-}$ hearts. Scale bars = 2 mm. (*B*) Optical action potentials (OAPs) from the initial pacemaker site in the SAN region (white asterisk on activation map) and earliest right atrial activation site (black asterisk on activation map) from WT (left) and NPR-B$^{+/-}$ (right) mice. These optical APs were used to quantify SAN to atrial conduction time (SACT). (*C–F*) Summary of atrial preparation beating rate (*C*), SACT (*D*), SAN conduction velocity (CV; *E*), frequency distribution of CV in the SAN (*F*) and optical APD_{50} (*G*) for WT ($n = 12$) and NPR-B$^{+/-}$ ($n = 12$) hearts. For (*C,D,G*), *$P < 0.001$ vs. WT by Student's *t*-test. For (*E*), *$P < 0.001$ vs. WT by Mann–Whitney *U* test.

that was due to PDE3 in wildtype and NPR-B$^{+/-}$ mice. PDE3 activity in the SAN was increased in NPR-B$^{+/-}$ mice compared to wildtype controls (*Figure 5B*) while PDE2 and PDE4 activity were not different (*Figure 5B*). Consistent with increased PDE3 activity, intracellular cAMP was lower in SAN myocytes isolated from NPR-B$^{+/-}$ mice (*Figure 5C*). Exogenous application of CNP (100 nM) increased cAMP concentrations in SAN myocytes from wildtype and NPR-B$^{+/-}$; however, overall cAMP concentrations remained lower in NPR-B$^{+/-}$ mice (*Figure 5C*). Conversely, inhibition of PDE3 with milrinone (10 μM) increased cAMP concentration in both genotypes and abolished the differences in SAN cAMP concentrations between wildtype and NPR-B$^{+/-}$ mice (*Figure 5C*). There were no differences in plasma CNP levels (*Figure 5D*) or in plasma cGMP levels

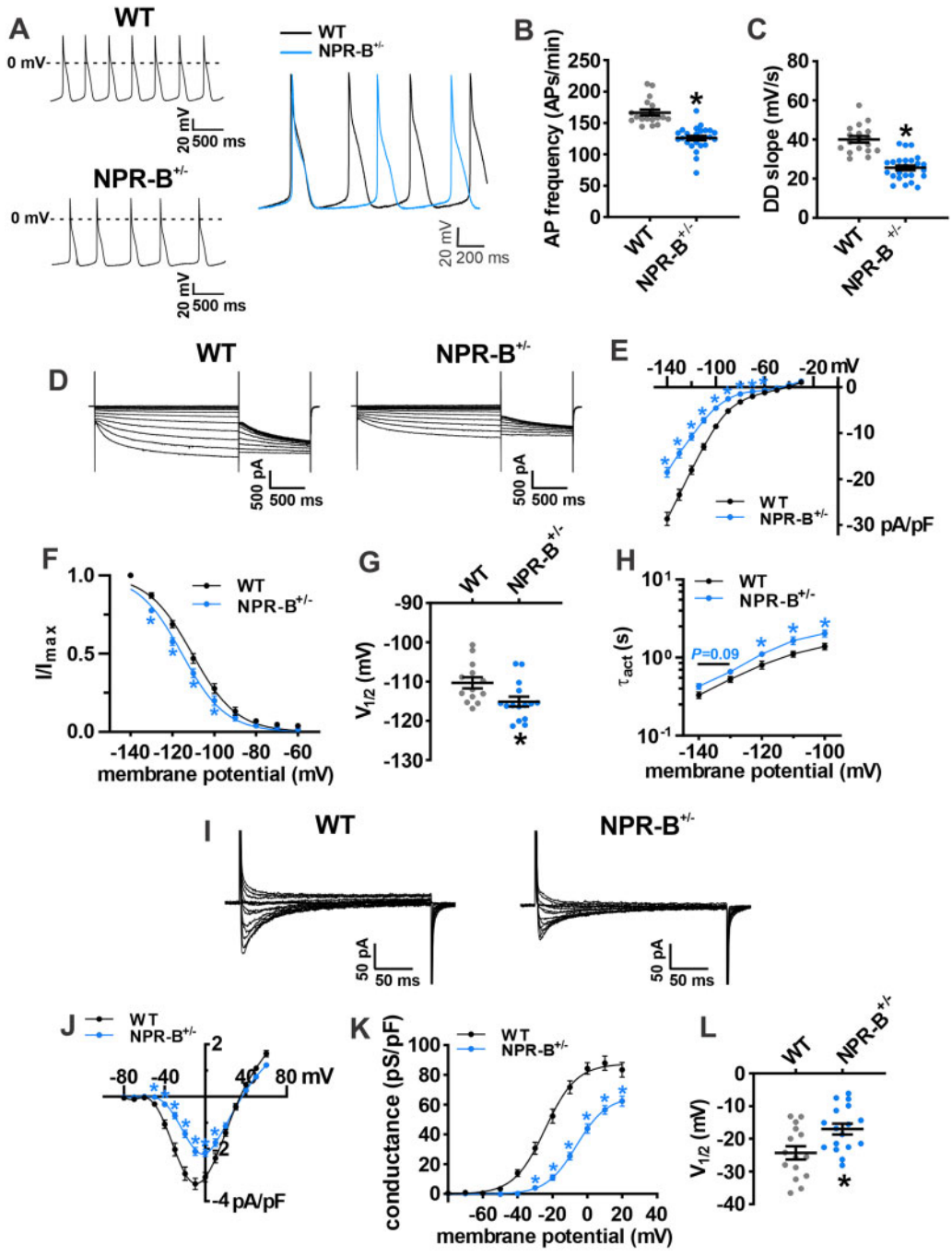

Figure 4 SAN myocyte electrophysiology in NPR-B$^{+/-}$ mice. (*A*) Representative spontaneous AP recordings in isolated SAN myocytes from WT and NPR-B$^{+/-}$ mice. (*B,C*) Summary of AP firing rate (*B*) and DD slope (*C*) in isolated SAN myocytes from WT ($n = 18$ cells from six mice) and NPR-B$^{+/-}$ ($n = 26$ cells from 10 mice) mice. *$P < 0.0001$ vs. WT by Student's *t*-test. See Supplementary material online, *Table S1* for additional AP parameters. (*D*) Representative I_f recordings in SAN myocytes isolated from WT and NPR-B$^{+/-}$ mice. (*E–G*), Summary I_f IV curves (*E*), activation curves (*F*), $V_{1/2}$ activation (*G*), and time constant of activation (τ_{act}; *H*) for WT ($n = 13$ cells from seven mice) and NPR-B$^{+/-}$ ($n = 15$ cells from six mice) mice. (*I*) Representative $I_{Ca,L}$ recordings in SAN myocytes isolated from WT and NPR-B$^{+/-}$ mice. (*J–L*) Summary $I_{Ca,L}$ IV curves (*J*), activation curves (*K*), and $V_{1/2}$ activation (*L*) for WT ($n = 15$ cells from six mice) and NPR-B$^{+/-}$ ($n = 17$ cells from six mice) mice. For (*E,F,H,J,K*), *$P < 0.01$ vs. WT at each membrane potential by two-way repeated-measures ANOVA with Holm–Sidak *post hoc* test. For panels G and K *$P < 0.05$ vs. WT by Student's *t*-test.

(*Figure 5E*) in NPR-B$^{+/-}$ mice. The mRNA expression of PDE3A and other PDEs in the SAN, as well as in the right atrium and left ventricle, where not different in NPR-B$^{+/-}$ mice (Supplementary material online, *Figure S14*). There were also no differences in intracellular cAMP in the right atrium or left ventricle (Supplementary material online, *Figure S14*). Collectively, these data demonstrate that NPR-B deficiency lowers

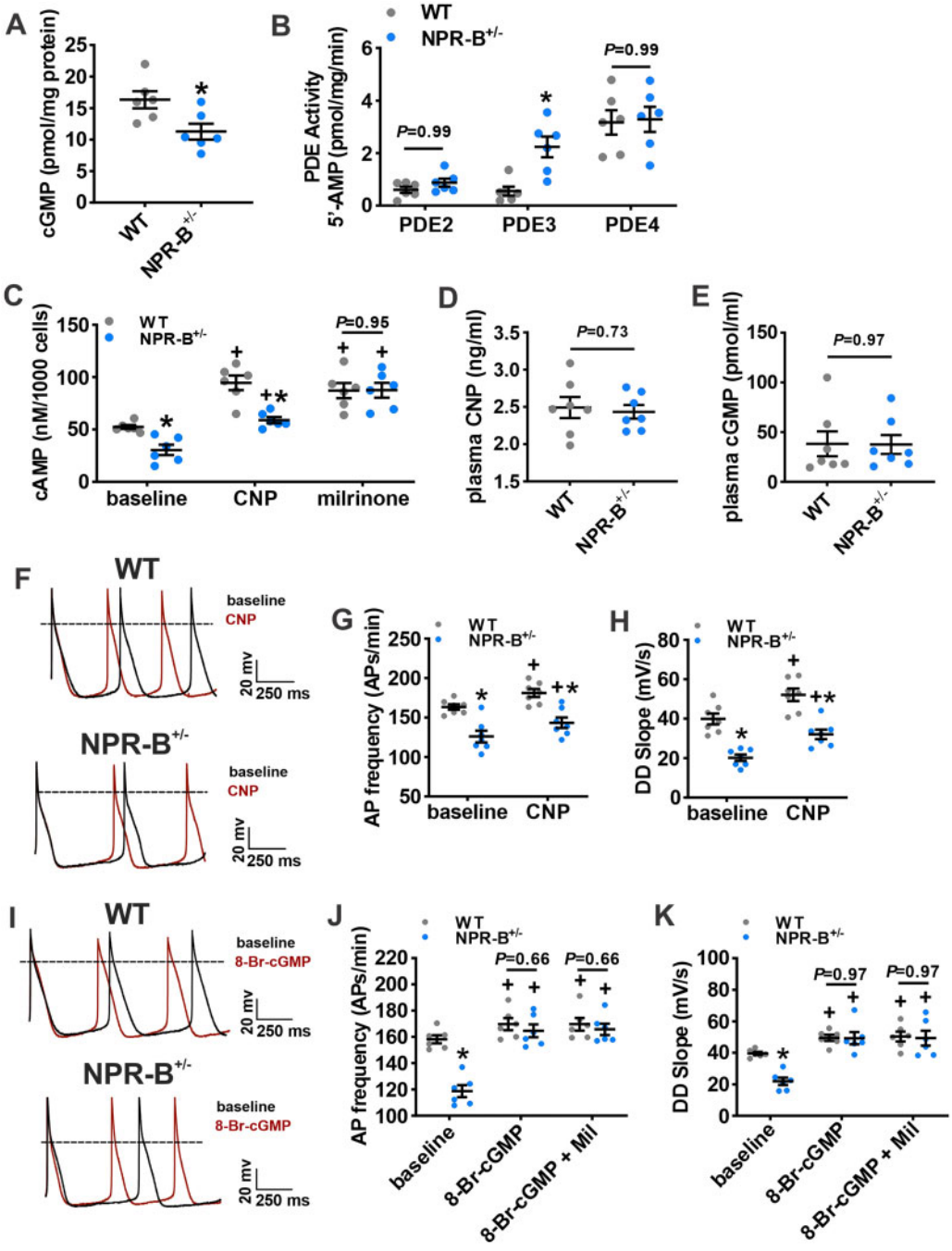

Figure 5 Altered cyclic nucleotide handling in the SAN of NPR-B$^{+/-}$ mice. (*A*) Whole atrial tissue cGMP levels in WT ($n = 6$ hearts) and NPR-B$^{+/-}$ ($n = 6$ hearts) mice. (*B*) Summary of phosphodiesterase 2, 3, and 4 (PDE2, PDE3, PDE4) activity in the SAN of WT and NPR-B$^{+/-}$ mice ($n = 6$ pooled SANs for each genotype). For (*A* and *B*), *$P < 0.05$ vs. WT by Student's *t*-test. (*C*) SAN myocyte intracellular cAMP production at baseline and in response to CNP (100 nM) or the PDE3 inhibitor milrinone (10 μM). $n = 6$ pooled SANs for each genotype; *$P < 0.05$ vs. WT within condition; $^{+}P < 0.05$ vs. baseline within genotype by two-way repeated-measures ANOVA with Holm–Sidak *post hoc* test. (*D*) Summary of plasma CNP in WT ($n = 7$) and NPR-B$^{+/-}$ ($n = 7$) mice. (*E*) Summary of plasma cGMP in WT ($n = 7$) and NPR-B$^{+/-}$ ($n = 7$) mice. (*D, E*) analysed by Student's *t*-test. (*F*) Representative spontaneous AP recordings in isolated SAN myocytes from WT and NPR-B$^{+/-}$ mice at baseline (black trace) and in response to CNP (100 nM; red trace). (*G,H*) Summary of the effects of CNP on spontaneous AP firing frequency (*G*) and DD slope (*H*) for WT ($n = 7$ cells from two mice) and NPR-B$^{+/-}$ ($n = 7$ cells from three mice) SAN myocytes. (*I*) Representative spontaneous AP recordings in isolated SAN myocytes from WT and NPR-B$^{+/-}$ mice at baseline (black trace) and in response intracellular dialysis of 8-Br-cGMP (10 μM; red trace). (*J, K*) Summary of the effects of 8-Br-cGMP and 8-Br-cGMP + Milrinone (Mil) on spontaneous AP firing frequency (*J*) and DD slope (*K*) in WT ($n = 6$ cells from six mice) and NPR-B$^{+/-}$ ($n = 6$ cells from five mice) SAN myocytes. For (*G, H, J*, and *K*) *$P < 0.05$ vs. WT within condition; $^{+}P < 0.05$ vs. baseline within genotype by two-way repeated-measures ANOVA with Holm–Sidak *post hoc* test.

intracellular cGMP levels leading to increased PDE3 activity and diminished cAMP signalling locally in the SAN.

3.7 Augmented cGMP levels restore regular SAN function in NPR-B deficient mice

Our results suggest that the reductions in HR observed in NPR-B deficient mice are due to lower levels of myocardial cGMP and increased PDE3 hydrolysis of cAMP in the SAN. To confirm this mechanism, we tested if enhancing intracellular cGMP signalling in SAN myocytes from NPR-B deficient mice would restore spontaneous SAN AP firing. Acute CNP (100 nM) application caused an increase in AP firing rate and DD slope in isolated SAN myocytes from both genotypes; however, AP firing frequency and DD slope remained reduced in NPR-B$^{+/-}$ mice (*Figure 5F–H*).

To bypass NPR-B and directly increase cGMP signalling SAN myocytes were dialysed with 8-Bromo-cGMP (8-Br-cGMP; 10 μM), a slowly hydrolyzed analogue of cGMP, via the patch pipette. 8-Br-cGMP increased spontaneous AP frequency and DD slope in SAN myocytes from both wildtype and NPR-B$^{+/-}$ mice to levels that no longer differed between genotypes (*Figure 5I–K*). Application of milrinone (10 μM) after 8-Br-cGMP dialysis did not cause any further increases in AP firing rate or DD slope in both groups suggesting that 8-Br-cGMP fully inhibited PDE3 in SAN myocytes (*Figure 5J,K*).

The effects of enhancing cGMP signalling on I_f and $I_{Ca,L}$ in NPR-B$^{+/-}$ SAN myocytes were also investigated (*Figure 6*; Supplementary material online, *Table S3*). I_f density was measured at -130 mV immediately after rupture during whole-cell recordings and after dialysis of 8-Br-cGMP (10 μM; *Figure 6A*). 8-Br-cGMP increased I_f density in SAN myocytes from both wildtype and NPR-B$^{+/-}$ mice and abolished the difference in I_f current density seen at baseline (*Figure 6B*). Summary IV curves demonstrate that 8-Br-cGMP normalized I_f density (*Figure 6C*) as well as I_f steady-state activation properties (*Figure 6D*; Supplementary material online, *Table S3*). 8-Br-cGMP also normalized the I_f time constants of activation (*Figure 6E*) in NPR-B$^{+/-}$ SAN myocytes.

Similarly, 8-Br-cGMP dialysis increased $I_{Ca,L}$ density in SAN myocytes from both wildtype and NPR-B$^{+/-}$ mice and abolished the differences in $I_{Ca,L}$ seen at baseline between genotypes (*Figure 6F,G*). Following 8-Br-cGMP application, summary $I_{Ca,L}$ IV curves did not differ between wildtype and NPR-B$^{+/-}$ mice (*Figure 6H*). $I_{Ca,L}$ activation properties from NPR-B$^{+/-}$ mice were also not different from wildtype controls (*Figure 6I*; Supplementary material online, *Table S3*).

$I_{Ca,L}$ has also been shown to be regulated by cGMP activated protein kinase G (PKG).[35] Accordingly, we next performed patch-clamp experiments to assess if the 8-Br-cGMP-stimulated increase in $I_{Ca,L}$ was due to enhanced activation of PKG in SAN myocytes. First, we examined the effects of the PKG inhibitor KT-5823 (0.5 μM) on basal $I_{Ca,L}$ in wildtype and NPR-B$^{+/-}$ mice (Supplementary material online, *Figure S15A,B*). As demonstrated previously, basal $I_{Ca,L}$ was reduced in NPR-B$^{+/-}$ mice compared to wildtype controls. Application of KT-5823 had no effect on $I_{Ca,L}$ current density in either wildtype or NPR-B$^{+/-}$ mice (Supplementary material online, *Figure S15B*). Additionally, we observed no effect of KT-5823 on 8-Br-cGMP stimulated increases in $I_{Ca,L}$ (Supplementary material online, *Figure S15C,D*). 8-Br-cGMP increased $I_{Ca,L}$ in both groups and abolished the differences in $I_{Ca,L}$ between wildtype and NPR-B$^{+/-}$ mice seen at baseline. Further application of KT-5823 had no effect on $I_{Ca,L}$ in either group suggesting that the effects of 8-Br-cGMP are not mediated through PKG.

Finally, the effects of milrinone (10 μM) on SAN conduction patterns were assessed using optical mapping (*Figure 7*). Activation maps (*Figure 7A*) and optical AP measurements (*Figure 7B*) demonstrate that milrinone increased beating rate (*Figure 7C*), increased conduction velocity in the SAN region in the right atrial posterior wall (*Figure 7D*) and decreased SACT (*Figure 7E*) to values that did not differ between wildtype and NPR-B$^{+/-}$ mice. These data demonstrate that the increase in PDE3 activity it the SAN accounts for impaired SAN function in NPR-B$^{+/-}$ mice.

4. Discussion

In the present study, we have identified a critical functional role for NPR-B in maintaining normal intrinsic SAN automaticity and in the physiological regulation of HR *in vivo*. Our findings demonstrate that NPR-B deficiency in mice results in reduced HR, impaired SAN conduction, and altered electrophysiological properties of SAN myocytes due to impaired cGMP-dependent regulation of I_f and $I_{Ca,L}$ by PDE3. These findings are highly consistent with clinical data in humans showing that heterozygous loss of function mutations in the NPR-B gene result in lower HRs compared to non-carrier family members.[18] Similarly, a recent study demonstrated that cardiac-specific deletion of CNP in mice results in reduced HR,[36] supporting the conclusion that CNP-mediated NPR-B signalling contributes to the maintenance of normal HR and SAN function under physiological conditions. NPs are best known for their ability to regulate cardiovascular homeostasis via their effects on blood pressure and blood volume.[10] Here we show that NPR-B-mediated cGMP signalling regulates HR via direct effects in the SAN and that this is a physiological determinant of HR regulation *in vivo*. Thus, our study provides new insight into the mechanisms by which NP signalling can regulate cardiac performance via NPR-B in the SAN.

Our study shows that awake and freely moving NPR-B$^{+/-}$ mice exhibit reduced HR *in vivo* during both phases of the diurnal cycle, following administration of ANS blockers, and during β-adrenergic receptor stimulation. There were no differences in activity level in NPR-B$^{+/-}$ mice. This indicates that the reductions in HR observed in NPR-B$^{+/-}$ mice were associated with impaired intrinsic SAN function and were independent of the ANS suggesting a key role for NPR-B in the SAN itself. This is consistent with recent studies demonstrating that intrinsic SAN beating rate is a critical determinant of HRV *in vivo*.[23,37,38] Nevertheless, previous studies have also identified a role for NP signalling and NPR-B in regulating sympathetic and parasympathetic nervous system activity leading to changes in HR.[13,29,39] For example, transgenic rats with neuronal-specific dominant-negative overexpression of NPR-B develop higher HRs and increased blood pressure due to elevated post-ganglionic sympathetic nerve activity.[39] CNP has also been shown to modulate vagal neurotransmission via presynaptic effects.[13] Conversely, in our model of global NPR-B deficiency, HR was reduced in association with increased HRV and increases in intrinsic SAN beating rate variability. Some of these differences could be related to the different models used in each study. The ability of CNP/NPR-B to affect HR via direct effects in the SAN as well as via effects on cardiac neurotransmission indicates site-specific NPR-B signalling is likely important and that, overall, NPR-B is a key regulator of HR.

SAN dysfunction in NPR-B$^{+/-}$ mice was evident as shown by increased cSNRT *in vivo*. Consistent with this, high-resolution optical mapping studies demonstrate that NPR-B$^{+/-}$ mice exhibited increased SAN conduction time and more inferior leading activation sites compared to WT

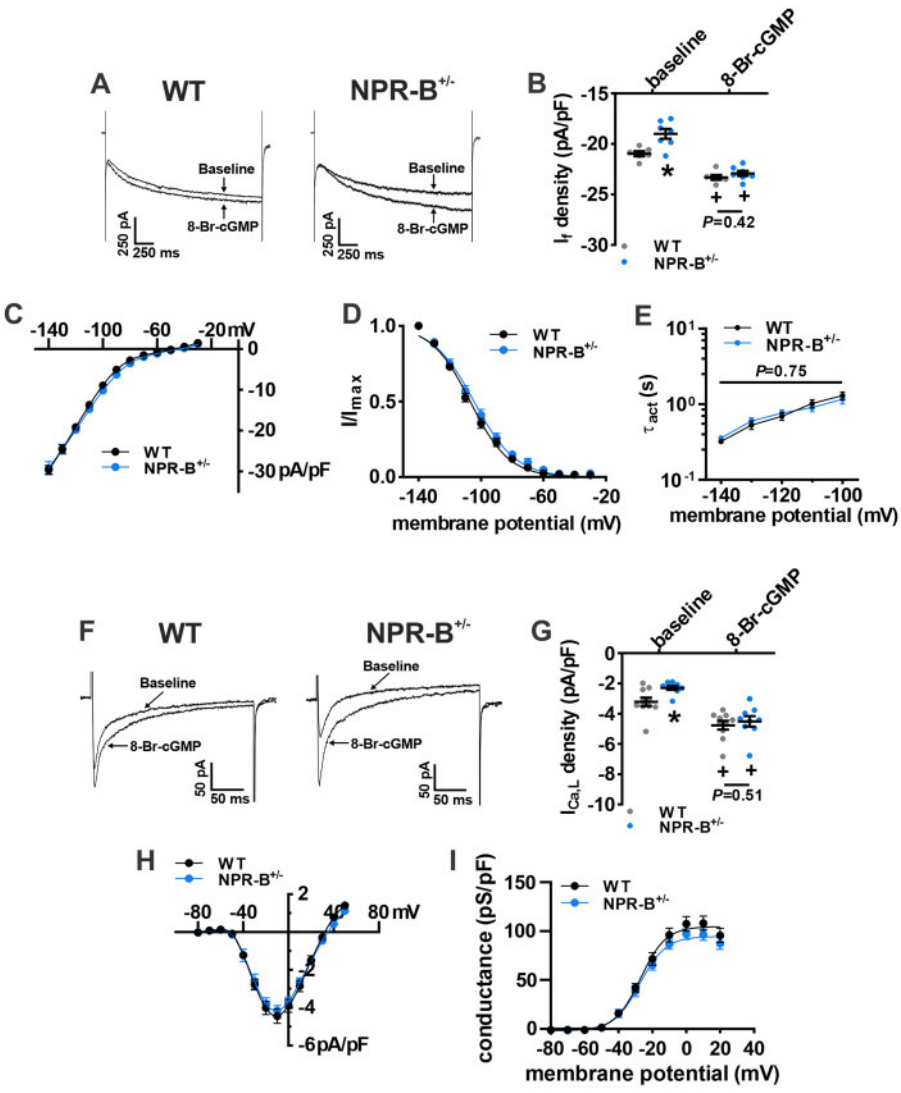

Figure 6 Effect of 8-Br-cGMP on I_f and $I_{Ca,L}$ in SAN myocytes from NPR-B$^{+/-}$ mice. (*A*) Representative I_f recordings (measured at –130 mV) at baseline and following intracellular dialysis of 8-Br-cGMP (10 μM) in isolated SAN myocytes from WT and NPR-B$^{+/-}$ mice. (*B*) Summary of the effects of 8-Br-cGMP on I_f density at –130 mV in WT ($n = 6$ cells from three mice) and NPR-B$^{+/-}$ ($n = 7$ cells from four mice) SAN myocytes. (*C–E*) Summary I_f IV curves (*C*), activation curves (*D*), and τ_{act} (*E*) for WT ($n = 10$ cells from six mice) and NPR-B$^{+/-}$ ($n = 9$ cells from five mice) SAN myocytes in the presence of 8-Br-cGMP. (*E*) Representative $I_{Ca,L}$ recordings (measured at –10 mV) at baseline and following intracellular dialysis of 8-Br-cGMP (10 μM) in isolated SAN myocytes from WT and NPR-B$^{+/-}$ mice. (*F*) Summary of the effects of 8-Br-cGMP on $I_{Ca,L}$ density at –10 mV in WT ($n = 10$ cells from three mice) and NPR-B$^{+/-}$ ($n = 9$ cells from two mice) SAN myocytes. (*G,H*) Summary $I_{Ca,L}$ IV curves (*G*) and activation curves (*H*) for WT ($n = 10$ cells from three mice) and NPR-B$^{+/-}$ ($n = 9$ cells from two mice) SAN myocytes in the presence of 8-Br-cGMP. For (*B, F*), $^*P < 0.05$ vs. WT within condition; $^+P < 0.05$ vs. baseline within genotype by two-way repeated-measures ANOVA with the Holm–Sidak *post hoc* test. For (*C, D, E, H,* and *I*) data analysed by two-way repeated-measures ANOVA with Holm–Sadak *post hoc* test.

mice. Inferior shifts in the leading activation site in the SAN, which can occur in disease states or following parasympathetic nervous system activation, are well known to be associated with lower HR.[22,32,40–42] In agreement with these findings, we have previously shown that acute exogenous application of CNP (the ligand for NPR-B) increases HR in association with superior shifts in leading activation site in the SAN.[12]

Impaired SAN function in NPR-B$^{+/-}$ mice occurred due to reductions in spontaneous AP firing and DD slope in SAN myocytes. These impairments were the result of reductions in I_f and $I_{Ca,L}$, which are critical regulators of SAN automaticity. Mechanistically, I_f and $I_{Ca,L}$ were reduced in association with shifts in the voltage dependence of activation ($V_{1/2(act)}$) for each current. These biophysical alterations were due to a reduction in intracellular cGMP and increased PDE3 activity, leading to a reduction in cAMP in the SAN in NPR-B$^{+/-}$ mice. Consistent with this, direct application of cGMP or milrinone (PDE3 inhibitor) normalized cAMP levels, AP firing, I_f and $I_{Ca,L}$ in SAN myocytes from NPR-B$^{+/-}$ mice while exogenous application of CNP did not. These findings indicate that impaired SAN function occurs due to reduced NPR-B levels and attenuated cGMP-mediated signalling downstream of this receptor in SAN myocytes. This is in agreement with previous studies showing that NPR-B

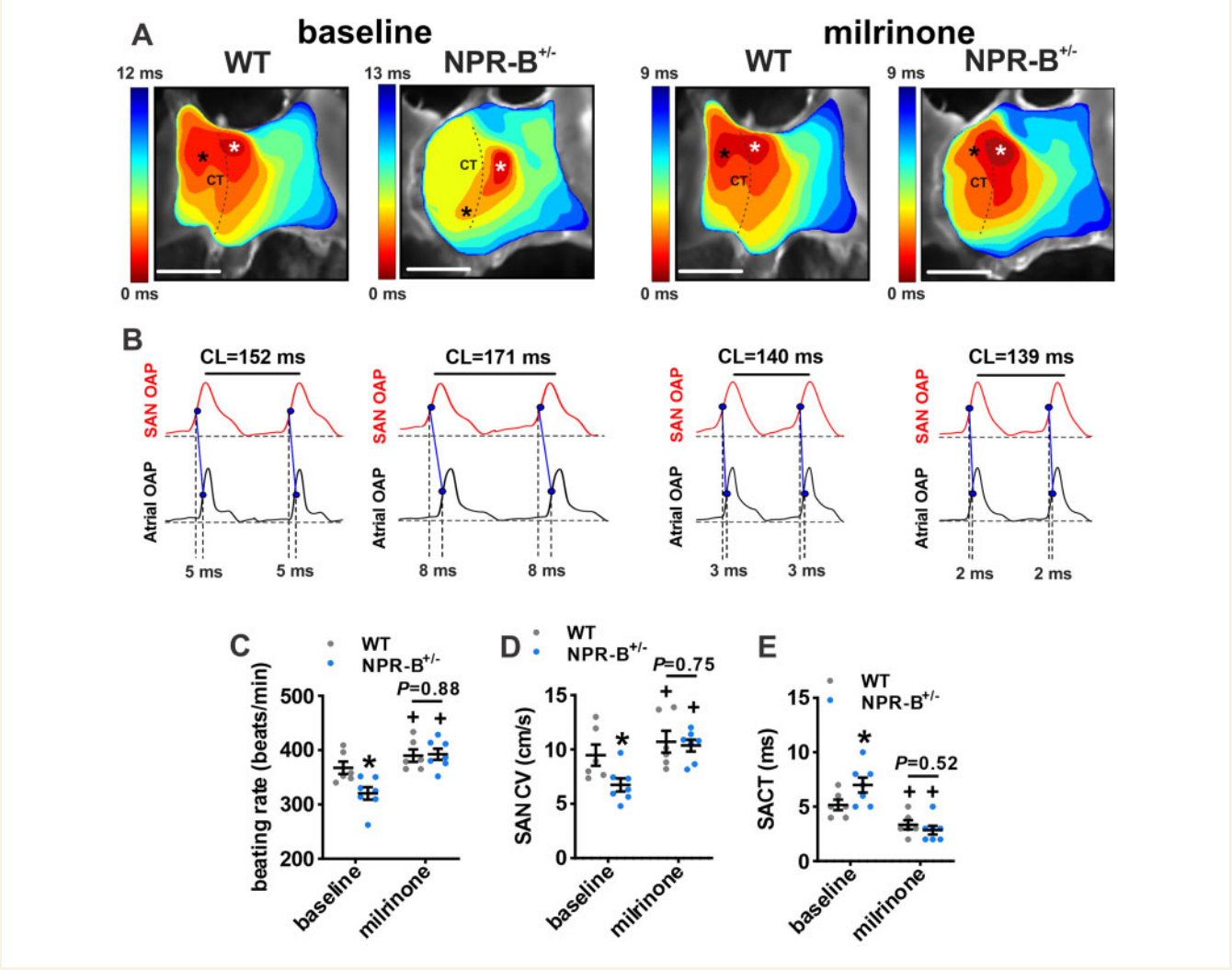

Figure 7 Effects of PDE3 inhibition on electrical conduction in the SAN in NPR-B$^{+/-}$ mice. (*A*) Representative activation maps for WT and NPR-B$^{+/-}$ hearts at baseline and after PDE3 inhibition with milrinone (10 μM). Scale bars = 2 mm. (*B*) Optical action potentials (OAPs) from the initial pacemaker site in the SAN region (white asterisk on activation maps) and earliest right atrial activation site (black asterisk on activation maps) from WT and NPR-B$^{+/-}$ hearts at baseline and in the presence of milrinone. Dashed lines illustrate SACT for these examples. (*C–E*) Summary of atrial preparation beating rate (*C*), SAN conduction velocity (CV; *D*), and SACT (*E*) for WT ($n = 6$) and NPR-B$^{+/-}$ ($n = 7$) hearts at baseline and after application of milrinone. For (*C–E*), *$P < 0.05$ vs. WT; $^{+}P < 0.05$ vs. baseline by two-way repeated measures ANOVA with Holm–Sidak *post hoc* test.

deficiency in rats results in lower cardiomyocyte cGMP generation[43] while HEK293A cells with a gain of function mutation in NPR-B exhibit elevated intracellular cGMP.[44] Thus, our study demonstrates that NPR-B regulates SAN AP firing via the cross-talk between cGMP and cAMP via PDE3. PDE3-dependent cAMP signalling is a critical determinant of SAN AP firing.[33,34,45] Reduced HR and impaired intrinsic SAN function in NPR-B$^{+/-}$ mice is consistent with previous studies demonstrating that acute application of exogenous CNP can increase HR, SAN conduction and SAN AP firing via PDE3.[11–14,46] We did not observe alterations in I_{Na} or Cx expression in the SAN of NPR-B$^{+/-}$ mice suggesting that conduction abnormalities and reduced HR are associated with the slower rate of diastolic depolarization due to reductions in I_f and $I_{Ca,L}$ identified in this study.

In addition to inhibiting PDE3, cGMP can also activate PDE2; however, it requires higher concentrations of cGMP to activate PDE2 than to inhibit PDE3.[7] PDE2 activity was not altered in the SAN in NPR-B$^{+/-}$ mice indicating that the reduction in cGMP in the SAN of NPR-B$^{+/-}$ mice was not able to alter PDE2 activity. PDE4 is not directly modulated by cGMP, but is importantly involved in cAMP hydrolysis.[7] Nevertheless, PDE4 activity was also not altered in NPR-B$^{+/-}$ mice. cGMP can also activate PKG,[47,48] which has been shown to modulate $I_{Ca,L}$ density in atrial and ventricular myocytes.[49–51] We found that there was no effect of PKG inhibition on basal $I_{Ca,L}$ or 8-Br-cGMP stimulated increases in $I_{Ca,L}$ in SAN myocytes. This is consistent with previous literature showing that the HR response to GC stimulation by nitric oxide donors is significantly reduced following PKA inhibition, but not PKG inhibition.[52] It is also conceivable that cGMP could directly affect HCN activation kinetics; however, while both cAMP and cGMP can enhance the activity of HCN channels,[53] the apparent affinities of HCN channels for cAMP are about 10-fold higher than for cGMP.[54] This, in conjunction with the low levels of cGMP (~10 nM) in adult cardiomyocytes compared to cAMP (~1 μM), would suggest that the direct action of cGMP on HCN channel activation in the SAN is relatively minimal. Thus, while cGMP can activate

a number of signalling pathways, our data show that cAMP levels in the SAN were normalized by milrinone and that SAN AP firing, DD slope, and SAN conduction properties were normalized by 8-Br-cGMP and milrinone in NPR-B$^{+/-}$ mice. From these data, we conclude that that the primary effect of NPR-B-mediated cGMP signalling in the SAN is via the inhibition of PDE3 and a subsequent increase in cAMP, which modulates the biophysical properties of key ionic currents (I_f and $I_{Ca,L}$) in SAN myocytes.

There was no evidence of hypertension or left ventricular dysfunction in NPR-B$^{+/-}$ mice in our study. We also found that SAN fibrosis was unchanged in NPR-B$^{+/-}$ mice. These observations are consistent with previous studies showing young NPR-B$^{-/-}$ mice are normotensive, with normal ventricular structure and function and normal ventricular fibrosis.[36] Previous studies have also shown that ventricular fibrosis is unchanged in NPR-B dominant-negative rats.[43] On the other hand, aged NPR-B deficient mice have been shown to develop ventricular hypertrophy and fibrosis[17] indicating loss of NPR-B may lead to further alterations with aging. We also observed no changes in expression of mRNAs or proteins for I_f and $I_{Ca,L}$ in the SAN of NPR-B$^{+/-}$ mice. Thus, our findings demonstrate that reduced HR and impaired SAN function in NPR-B$^{+/-}$ mice are not associated with pathological cardiac remodelling or changes in ion channel expression. Rather, these data, in conjunction with our electrophysiological and molecular studies, indicate that the alterations in SAN function in NPR-B$^{+/-}$ occur due to the loss of normal physiological signalling via CNP due to reduced NPR-B levels and NPR-B that acts to maintain normal SAN function. These findings demonstrate an essential physiological role for the regulation of HR and intrinsic SAN function by CNP via NPR-B signalling and the modulation of ion channel function in SAN myocytes. We observed no changes in plasma CNP or cGMP concentrations despite reduced cGMP in the SAN. These findings agree with the hypothesis that CNP can elicit localized effects within the heart, including in a paracrine fashion and support the conclusion that impaired SAN function in NPR-B$^{+/-}$ mice occur due to impaired cGMP-mediated signalling secondary to reduced NPR-B expression in SAN myocytes rather than a change in CNP availability. Despite reduced expression of NPR-B in the atria and ventricles, there were no differences in atrial and ventricular cAMP levels and there was no evidence of changes in conduction from the atria to the ventricles in NPR-B$^{+/-}$ mice, based on analysis of AH and HV intervals. The relative expression of NPR-B is approximately two-fold higher in the SAN compared to the left ventricle.[21] Similarly, adenylyl cyclase activity and PDE3 activity are high in the SAN compared to the working myocardium.[11,33,45,55] These factors may partially account for the impact of NPR-B deficiency on HR and SAN function with an absence of alterations in ventricular function.

In addition to activating NPR-B, CNP can also activate the NPR-C receptor.[9] We previously showed that NPR-C knockout mice also exhibit SAN dysfunction; however, this occurred via distinct mechanisms from those observed in the present study in NPR-B$^{+/-}$ mice. Specifically, SAN dysfunction in NPR-C knockout mice occurred due to enhanced SAN fibrosis without alterations in SAN AP firing and AP morphology.[21,22] These findings suggest that CNP can maintain SAN function via NPR-B-mediated effects on ion channel function as well as via NPR-C-mediated effects on SAN fibrosis. This highlights the importance of the NP system in maintaining HR and SAN function and suggests that multiple NPRs are involved in these effects. There were no changes in expression of other NPRs (i.e. NPR-A and NPR-C) in the SAN in NPR-B$^{+/-}$ mice indicating that the alterations in SAN function identified in the present study are the direct result of loss of NPR-B function.

Some limitations of our study should be noted. SAN function and regulation of ion channels by PDEs in mice may exhibit differences compared to humans. Investigating the mechanisms identified in our study in large animal models and ultimately humans will be necessary in future studies. In addition, our study focused on I_f and $I_{Ca,L}$, which are critical ionic currents involved in pacemaker function in the SAN. Nevertheless, other mechanisms such as sarcoplasmic reticulum (SR) Ca^{2+} release and the Na^{+}-Ca^{2+} exchanger also contribute to DD slope generation and spontaneous AP firing.[56,57] Furthermore, ion channel function and SR Ca^{2+} handling are linked such that effects on L-type Ca^{2+} channels may lead to downstream of effects on SR Ca^{2+} handling. Whether these other currents and pacemaker mechanisms are regulated by cAMP and PKA downstream of NPR-B is not known and requires further investigation. HR is a major determinant of cardiac output; however, cardiac output was not directly assessed in the present study. qPCR and Western blot studies were performed in whole tissues that will contain myocytes as well as other cell types, such as fibroblasts and neurons. Our study used mice with global NPR-B$^{+/-}$ deficiency; however, the degree of reduction of NPR-B in SAN myocytes compared to other tissues such as autonomic ganglia was not investigated. Finally, we did not use homozygous NPR-B knockout mice as these mice exhibit severe dwarfism[58] making them unsuitable for many of our experimental approaches. Nevertheless, using NPR-B$^{+/-}$ mice as a model of NPR-B deficiency, rather than complete loss of NPR-B, more closely mimics known human mutations associated with loss of NPR-B function.

5. Conclusion

Our multi-level assessment of HR and SAN function in NPR-B$^{+/-}$ mice provides novel mechanistic insight into the role of NPR-B in regulating SAN automaticity. This work demonstrates that NPR-B deficiency is associated with impaired SAN function due to altered cGMP-dependent effects on ion channel function in SAN myocytes. From these studies, we conclude that NPR-B-mediated cGMP signalling plays a fundamental role in maintaining normal HR and SAN function, thereby providing new insight into the critical role of endocrine/paracrine regulation of cardiovascular homeostasis by NPs. These findings have important implications for identifying mechanisms of SAN dysfunction and alterations in cardiac performance in conditions associated with altered NP signalling. These findings also suggest that NPR-B stimulators could be a novel approach for improving or maintaining SAN function in conditions associated with SAN disease, which will be an important area of ongoing study.

Supplementary material

Supplementary material is available at *Cardiovascular Research* online.

Authors' contributions

T.W.D. and R.A.R. contributed to conception and experimental design. T.W.D., H.J.J., and L.B.J. performed telemetry and intracardiac studies. T.W.D., M.M., and L.J.B. performed and analysed optical mapping experiments. T.W.D. performed and analysed all patch clamp experiments. M.M. and M.D.M. performed and analysed sinoatrial node histology. M.M., H.J.J., and L.A. performed qPCR. T.W.D. and Y.L. performed all western blots. D.D.B. performed and analysed echocardiography

experiments. T.W.D. and R.A.R. prepared the figures and wrote the manuscript. All authors contributed to editing the final version of the manuscript.

Funding

This work was supported by the Canadian Institutes of Health Research to R.A.R. (MOP 142486 and PJT 1666105). T.W.D. and M.M. each hold a Canadian Institutes of Health Research Doctoral Research Award. H.J.J. was supported by a Killam Postdoctoral Fellowship and a Libin Cardiovascular Institute Postdoctoral Fellowship. L.J.B. holds a Libin Cardiovascular Institute Doctoral Research Award. Y.L. holds a Canadian Institutes of Health Research Postdoctoral Fellowship.

Conflict of interest: none declared.

Data availability

The data supporting the findings of this study are available from the corresponding author upon reasonable request.

References

1. Mangoni ME, Nargeot J. Genesis and regulation of the heart automaticity. *Physiol Rev* 2008;**88**:919–982.
2. Bartos DC, Grandi E, Ripplinger CM. Ion channels in the heart. *Compr Physiol* 2015;**5**:1423–1464.
3. Lei M, Jones SA, Liu J, Lancaster MK, Fung SS, Dobrzynski H, Camelliti P, Maier SK, Noble D, Boyett MR. Requirement of neuronal- and cardiac-type sodium channels for murine sinoatrial node pacemaking. *J Physiol* 2004;**559**:835–848.
4. Lei M, Zhang H, Grace AA, Huang CL. SCN5A and sinoatrial node pacemaker function. *Cardiovasc Res* 2007;**74**:356–365.
5. Verheijck EE, van Kempen MJ, Veereschild M, Lurvink J, Jongsma HJ, Bouman LN. Electrophysiological features of the mouse sinoatrial node in relation to connexin distribution. *Cardiovasc Res* 2001;**52**:40–50.
6. MacDonald EA, Rose RA, Quinn TA. Neurohumoral control of sinoatrial node activity and heart rate: insight from experimental models and findings from humans. *Front Physiol* 2020;**11**:170
7. Bender AT, Beavo JA. Cyclic nucleotide phosphodiesterases: molecular regulation to clinical use. *Pharmacol Rev* 2006;**58**:488–520.
8. Moghtadaei M, Polina I, Rose RA. Electrophysiological effects of natriuretic peptides in the heart are mediated by multiple receptor subtypes. *Prog Biophys Mol Biol* 2016;**120**:37–49.
9. Rose RA, Giles WR. Natriuretic peptide C receptor signalling in the heart and vasculature. *J Physiol* 2008;**586**:353–366.
10. Potter LR, Abbey-Hosch S, Dickey DM. Natriuretic peptides, their receptors, and cyclic guanosine monophosphate-dependent signaling functions. *Endocr Rev* 2006;**27**:47–72.
11. Springer J, Azer J, Hua R, Robbins C, Adamczyk A, McBoyle S, Bissell MB, Rose RA. The natriuretic peptides BNP and CNP increase heart rate and electrical conduction by stimulating ionic currents in the sinoatrial node and atrial myocardium following activation of guanylyl cyclase-linked natriuretic peptide receptors. *J Mol Cell Cardiol* 2012;**52**:1122–1134.
12. Azer J, Hua R, Krishnaswamy PS, Rose RA. Effects of natriuretic peptides on electrical conduction in the sinoatrial node and atrial myocardium of the heart. *J Physiol* 2014;**592**:1025–1045.
13. Herring N, Zaman JA, Paterson DJ. Natriuretic peptides like NO facilitate cardiac vagal neurotransmission and bradycardia via a cGMP pathway. *Am J Physiol Heart Circ Physiol* 2001;**281**:H2318–2327.
14. Beaulieu P, Cardinal R, De Lean A, Lambert C. Direct chronotropic effects of atrial and C-type natriuretic peptides in anaesthetized dogs. *Br J Pharmacol* 1996;**118**:1790–1796.
15. Dickey DM, Flora DR, Bryan PM, Xu X, Chen Y, Potter LR. Differential regulation of membrane guanylyl cyclases in congestive heart failure: natriuretic peptide receptor (NPR)-B, Not NPR-A, is the predominant natriuretic peptide receptor in the failing heart. *Endocrinology* 2007;**148**:3518–3522.
16. Del Ry S, Cabiati M, Lionetti V, Emdin M, Recchia FA, Giannessi D. Expression of C-type natriuretic peptide and of its receptor NPR-B in normal and failing heart. *Peptides* 2008;**29**:2208–2215.
17. Blaser MC, Wei K, Adams RLE, Zhou YQ, Caruso LL, Mirzaei Z, Lam AY, Tam RKK, Zhang H, Heximer SP, Henkelman RM, Simmons CA. Deficiency of natriuretic peptide receptor 2 promotes bicuspid aortic valves, aortic valve disease, left ventricular dysfunction, and ascending aortic dilatations in mice. *Circ Res* 2018;**122**:405–416.
18. Olney RC, Bukulmez H, Bartels CF, Prickett TC, Espiner EA, Potter LR, Warman ML. Heterozygous mutations in natriuretic peptide receptor-B (NPR2) are associated with short stature. *J Clin Endocrinol Metab* 2006;**91**:1229–1232.
19. Sanders P, Kistler PM, Morton JB, Spence SJ, Kalman JM. Remodeling of sinus node function in patients with congestive heart failure: reduction in sinus node reserve. *Circulation* 2004;**110**:897–903.
20. Urena M, Hayek S, Cheema AN, Serra V, Amat-Santos IJ, Nombela-Franco L, Ribeiro HB, Allende R, Paradis J-M, Dumont E, Thourani VH, Babaliaros V, Francisco Pascual J, Cortés C, Del Blanco BG, Philippon F, Lerakis S, Rodés-Cabau J. Arrhythmia burden in elderly patients with severe aortic stenosis as determined by continuous electrocardiographic recording: toward a better understanding of arrhythmic events after transcatheter aortic valve replacement. *Circulation* 2015;**131**:469–477.
21. Egom EE, Vella K, Hua R, Jansen HJ, Moghtadaei M, Polina I, Bogachev O, Hurnik R, Mackasey M, Rafferty S, Ray G, Rose RA. Impaired sinoatrial node function and increased susceptibility to atrial fibrillation in mice lacking natriuretic peptide receptor C. *J Physiol* 2015;**593**:1127–1146.
22. Mackasey M, Egom EE, Jansen HJ, Hua R, Moghtadaei M, Liu Y, Kaur J, McRae MD, Bogachev O, Rafferty SA, Ray G, Kirkby AW, Rose RA. Natriuretic peptide receptor-C protects against angiotensin II-mediated sinoatrial node disease in mice. *JACC Basic Transl Sci* 2018;**3**:824–843.
23. Dorey TW, Moghtadaei M, Rose RA. Altered heart rate variability in angiotensin II-mediated hypertension is associated with impaired autonomic nervous system signaling and intrinsic sinoatrial node dysfunction. *Heart Rhythm* 2020;**17**:1360–1370.
24. Moghtadaei M, Langille E, Rafferty SA, Bogachev O, Rose RA. Altered heart rate regulation by the autonomic nervous system in mice lacking natriuretic peptide receptor C (NPR-C). *Sci Rep* 2017;**7**:17564.
25. Moghtadaei M, Jansen HJ, Mackasey M, Rafferty SA, Bogachev O, Sapp JL, Howlett SE, Rose RA. The impacts of age and frailty on heart rate and sinoatrial node function. *J Physiol* 2016;**594**:7105–7126.
26. Jansen HJ, Mackasey M, Moghtadaei M, Liu Y, Kaur J, Egom EE, Tuomi JM, Rafferty SA, Kirkby AW, Rose RA. NPR-C (natriuretic peptide receptor-C) modulates the progression of angiotensin ii-mediated atrial fibrillation and atrial remodeling in mice. *Circ Arrhythm Electrophysiol* 2019;**12**:e006863.
27. Jansen HJ, Mackasey M, Moghtadaei M, Belke DD, Egom EE, Tuomi JM, Rafferty SA, Kirkby AW, Rose RA. Distinct patterns of atrial electrical and structural remodeling in angiotensin II mediated atrial fibrillation. *J Mol Cell Cardiol* 2018;**124**:12–25.
28. Jensen PN, Gronroos NN, Chen LY, Folsom AR, deFilippi C, Heckbert SR, Alonso A. Incidence of and risk factors for sick sinus syndrome in the general population. *J Am Coll Cardiol* 2014;**64**:531–538.
29. Ajijola OA, Shivkumar K, Habecker BA. Natriuretic peptides and peripheral autonomic neurotransmission: back to the A, B, and C's. *Cardiovasc Res* 2016;**112**:619–621.
30. Yaniv Y, Lyashkov AE, Lakatta EG. The fractal-like complexity of heart rate variability beyond neurotransmitters and autonomic receptors: signaling intrinsic to sinoatrial node pacemaker cells. *Cardiovasc Pharm Open Access* 2013;**2**:111.
31. Monfredi O, Lyashkov AE, Johnsen AB, Inada S, Schneider H, Wang R, Nirmalan M, Wisloff U, Maltsev VA, Lakatta EG, Zhang H, Boyett MR. Biophysical characterization of the underappreciated and important relationship between heart rate variability and heart rate. *Hypertension* 2014;**64**:1334–1343.
32. Krishnaswamy PS, Egom EE, Moghtadaei M, Jansen HJ, Azer J, Bogachev O, Mackasey M, Robbins C, Rose RA. Altered parasympathetic nervous system regulation of the sinoatrial node in Akita diabetic mice. *J Mol Cell Cardiol* 2015;**82**:125–135.
33. Hua R, Adamczyk A, Robbins C, Ray G, Rose RA. Distinct patterns of constitutive phosphodiesterase activity in mouse sinoatrial node and atrial myocardium. *PLoS One* 2012;**7**:e47652.
34. Vinogradova TM, Sirenko S, Lukyanenko YO, Yang D, Tarasov KV, Lyashkov AE, Varghese NJ, Li Y, Chakir K, Ziman B, Lakatta EG. Basal spontaneous firing of rabbit sinoatrial node cells is regulated by dual activation of PDEs (phosphodiesterases) 3 and 4. *Circ Arrhythm Electrophysiol* 2018;**11**:e005896.
35. Mahapatra S, Marcantoni A, Zuccotti A, Carabelli V, Carbone E. Equal sensitivity of Cav1.2 and Cav1.3 channels to the opposing modulations of PKA and PKG in mouse chromaffin cells. *J Physiol* 2012;**590**:5053–5073.
36. Moyes AJ, Chu SM, Aubdool AA, Dukinfield MS, Margulies KB, Bedi KC, Hodivala-Dilke K, Baliga RS, Hobbs AJ. C-type natriuretic peptide co-ordinates cardiac structure and function. *Eur Heart J* 2020;**41**:1006–1020.
37. Yaniv Y, Lyashkov AE, Lakatta EG. Impaired signaling intrinsic to sinoatrial node pacemaker cells affects heart rate variability during cardiac disease. *J Clin Trials* 2014;**4**:152.
38. Papaioannou VE, Verkerk AO, Amin AS, de Bakker JM. Intracardiac origin of heart rate variability, pacemaker funny current and their possible association with critical illness. *Curr Cardiol Rev* 2013;**9**:82–96.
39. Buttgereit J, Shanks J, Li D, Hao G, Athwal A, Langenickel TH, Wright H, da Costa Goncalves AC, Monti J, Plehm R, Popova E, Qadri F, Lapidus I, Ryan B, Ozcelik C, Paterson DJ, Bader M, Herring N. C-type natriuretic peptide and natriuretic peptide

receptor B signalling inhibits cardiac sympathetic neurotransmission and autonomic function. *Cardiovasc Res* 2016;**112**:637–644.
40. Fedorov VV, Hucker WJ, Dobrzynski H, Rosenshtraukh LV, Efimov IR. Postganglionic nerve stimulation induces temporal inhibition of excitability in rabbit sinoatrial node. *Am J Physiol Heart Circ Physiol* 2006;**291**:H612–623.
41. Glukhov AV, Fedorov VV, Anderson ME, Mohler PJ, Efimov IR. Functional anatomy of the murine sinus node: high-resolution optical mapping of ankyrin-B heterozygous mice. *Am J Physiol Heart Circ Physiol* 2010;**299**:H482–491.
42. Bleeker WK, Mackaay AJ, Masson-Pevet M, Bouman LN, Becker AE. Functional and morphological organization of the rabbit sinus node. *Circ Res* 1980;**46**:11–22.
43. Langenickel TH, Buttgereit J, Pagel-Langenickel I, Lindner M, Monti J, Beuerlein K, Al-Saadi N, Plehm R, Popova E, Tank J, Dietz R, Willenbrock R, Bader M. Cardiac hypertrophy in transgenic rats expressing a dominant-negative mutant of the natriuretic peptide receptor B. *Proc Natl Acad Sci USA* 2006;**103**:4735–4740.
44. Miura K, Namba N, Fujiwara M, Ohata Y, Ishida H, Kitaoka T, Kubota T, Hirai H, Higuchi C, Tsumaki N, Yoshikawa H, Sakai N, Michigami T, Ozono K. An overgrowth disorder associated with excessive production of cGMP due to a gain-of-function mutation of the natriuretic peptide receptor 2 gene. *PLoS One* 2012;**7**:e42180.
45. Vinogradova TM, Sirenko S, Lyashkov AE, Younes A, Li Y, Zhu W, Yang D, Ruknudin AM, Spurgeon H, Lakatta EG. Constitutive phosphodiesterase activity restricts spontaneous beating rate of cardiac pacemaker cells by suppressing local Ca2+ releases. *Circ Res* 2008;**102**:761–769.
46. Beaulieu P, Cardinal R, Page P, Francoeur F, Tremblay J, Lambert C. Positive chronotropic and inotropic effects of C-type natriuretic peptide in dogs. *Am J Physiol* 1997; **273**:H1933–1940.
47. Feil R, Lohmann SM, de Jonge H, Walter U, Hofmann F. Cyclic GMP-dependent protein kinases and the cardiovascular system: insights from genetically modified mice. *Circ Res* 2003;**93**:907–916.
48. Lohmann SM, Fischmeister R, Walter U. Signal transduction by cGMP in heart. *Basic Res Cardiol* 1991;**86**:503–514.
49. Wang Y, Wagner MB, Joyner RW, Kumar R. cGMP-dependent protein kinase mediates stimulation of L-type calcium current by cGMP in rabbit atrial cells. *Cardiovasc Res* 2000;**48**:310–322.
50. Vandecasteele G, Verde I, Rucker-Martin C, Donzeau-Gouge P, Fischmeister R. Cyclic GMP regulation of the L-type Ca(2+) channel current in human atrial myocytes. *J Physiol* 2001;**533**:329–340.
51. Kumar R, Namiki T, Joyner RW. Effects of cGMP on L-type calcium current of adult and newborn rabbit ventricular cells. *Cardiovasc Res* 1997;**33**:573–582.
52. Musialek P, Rigg L, Terrar DA, Paterson DJ, Casadei B. Role of cGMP-inhibited phosphodiesterase and sarcoplasmic calcium in mediating the increase in basal heart rate with nitric oxide donors. *J Mol Cell Cardiol* 2000;**32**:1831–1840.
53. Kaupp UB, Seifert R. Molecular diversity of pacemaker ion channels. *Annu Rev Physiol* 2001;**63**:235–257.
54. Craven KB, Zagotta WN. CNG and HCN channels: two peas, one pod. *Annu Rev Physiol* 2006;**68**:375–401.
55. Vinogradova TM, Lyashkov AE, Zhu W, Ruknudin AM, Sirenko S, Yang D, Deo S, Barlow M, Johnson S, Caffrey JL, Zhou YY, Xiao RP, Cheng H, Stern MD, Maltsev VA, Lakatta EG. High basal protein kinase A-dependent phosphorylation drives rhythmic internal Ca2+ store oscillations and spontaneous beating of cardiac pacemaker cells. *Circ Res* 2006;**98**:505–514.
56. Lakatta EG, Maltsev VA, Vinogradova TM. A coupled SYSTEM of intracellular Ca2+ clocks and surface membrane voltage clocks controls the timekeeping mechanism of the heart's pacemaker. *Circ Res* 2010;**106**:659–673.
57. Neco P, Rose B, Huynh N, Zhang R, Bridge JH, Philipson KD, Goldhaber JI. Sodium-calcium exchange is essential for effective triggering of calcium release in mouse heart. *Biophys J* 2010;**99**:755–764.
58. Tamura N, Doolittle LK, Hammer RE, Shelton JM, Richardson JA, Garbers DL. Critical roles of the guanylyl cyclase B receptor in endochondral ossification and development of female reproductive organs. *Proc Natl Acad Sci USA* 2004;**101**: 17300–17305.

Translational perspective

Natriuretic peptides are critical regulators of cardiac function. We report that natriuretic peptide receptor B (NPR-B) deficiency results in reduced heart rate due to impaired sinoatrial node (SAN) function. These effects are due in part to alterations in SAN ion channel function, including I_f and $I_{Ca,L}$, in association with reduced cGMP and alterations in cAMP regulation via phosphodiesterase 3 in the SAN. These data demonstrate that NPR-B plays an essential functional role in maintaining normal heart rate and SAN function suggesting that NPR-B may be a novel target for regulating HR clinically.

Natriuretic peptide receptor B maintains heart rate and sinoatrial node function via cyclic GMP mediated signaling

Supplemental Material

Supplemental Methods

Animals

This study used male and female wildtype and NPR-B$^{+/-}$ mice at 20 weeks of age. NPR-B$^{+/-}$ mice were initially obtained from Jackson Laboratory (*Npr2*^{tm1Gar}*/J*; stock #007658) and backcrossed into the C57Bl/6 line. All experimental procedures were approved by the University of Calgary Animal Care and Use Committee or the Dalhousie University Committee for Laboratory Animals and were in accordance with the guidelines of the Canadian Council on Animal Care and the NIH guide for the care and use of laboratory animals.

Telemetric ECG recordings and heart rate variability analysis

Telemetric ECG recordings (HD-X11 telemeters, Data Sciences International) were used to measure HR and activity levels in conscious freely moving mice. ECG leads were positioned subcutaneously in a lead II position to continuously measure HR as we have previously described[1,2]. Baseline ECG was collected for 36 hrs following 3 weeks of surgical recovery. The effects of ANS blockade were investigated by intraperitoneal injection of the β-adrenergic receptor (β-AR) antagonist propranolol hydrochloride (10 mg/kg) and the muscarinic receptor antagonist atropine sulfate (10 mg/kg) alone, or in combination, to assess vagal and sympathetic tone as well as intrinsic SAN rate. A minimum of 24 hrs was provided between injections. ECGs were recorded continuously for 1 hr following drug injection. ECG data acquisition, ECG filtering and R-wave detection was done using PowerLab and LabChart (ADInstruments, V8). Heart rate variability (HRV), a surrogate marker for autonomic nervous system activity, was assessed by time (SDNN and RMSSD) and frequency domain analysis of the R-R intervals using a custom MATLAB script.[1] To correct these metrics for the effect of HR

on HRV, all SDNN data (collected during high and low activity) was plotted as a function of corresponding HR and fit with an exponential function in order to generate the following equation to correct for HR and produce corrected SDNN (cSDNN=SDNN/(e^(-0.007xHR)) data as we have previously described.[1] Heart rate variability was also assessed using non-linear metrics from Poincaré plot analysis as we have previously described.[2] From these plots the standard deviations (SD1 and SD2) were calculated using the following equations: $SD1^2=1/2[SD(RR_n-RR_{n+1})]^2$ and $SD2^2=2[SD(RR)]^2-1/2[SD(RR_n-RR_{n+1})]^2$.

***In vivo* electrophysiology**

HR was measured in anesthetized mice (2% isoflurane inhalation) using 30-gauge subdermal needle electrodes (Grass Technologies) to record body surface (lead II) ECGs. In parallel, a 1.2 French octapolar electrophysiology catheter was inserted in the right heart via the jugular vein and used for intracardiac programmed stimulation experiments, as we have described previously.[3,4] All stimulation pulses were given at 3 V for 2 ms, which enabled continuous capture and drive of cardiac conduction. Sinoatrial node recovery time (SNRT) was measured by delivering a 12-stimulus drive train at a cycle length of 100 ms. SNRT is defined as the time between the last stimulus in the drive train and the occurrence of the first spontaneous atrial beat (P wave). SNRT was corrected for heart rate (cSNRT) by subtracting the prestimulus RR interval from the measured SNRT. His bundle signals were used to quantify atrial-His (AH) and His-ventricular (HV) intervals. Data were acquired using a Gould ACQ-7700 amplifier and Ponemah Physiology Platform software (Data Sciences International). Body temperature was monitored continuously via a rectal probe and maintained at 37°C with a heating pad.

Echocardiography and Systolic Blood Pressure Assessment.

Cardiac structure and function were assessed in anesthetized mice (2% isoflurane inhalation) by using transthoracic echocardiography. Echocardiography was performed using a high-resolution Vevo 3100 ultrasound machine (Fujufilm VisualSonics) to measure 2-dimensional (2D) M-mode images from the parasternal short axis at the level of the midpapillary muscle, as we have described previously[3,4]. Systolic and diastolic blood pressure (SBP and DBP) were measured in conscious restrained mice using a tail cuff apparatus (IITC Life Sci)

High-resolution optical mapping

To investigate patterns of electrical conduction in the SAN we used high resolution optical mapping in atrial preparations as we have described previously.[5-8] Hearts were excised into Krebs solution (37°C) containing (in mM): 118 NaCl, 4.7 KCl, 1.2 KH_2PO_4, 25 $NaHCO_3$, 1 $CaCl_2$, 1 $MgCl_2$, 11 glucose and bubbled with 95% O_2/5% CO_2 to maintain a pH of 7.4. The atrial preparation was superfused continuously with Krebs solution (37°C) bubbled with 95% O_2/5% CO_2 and allowed to equilibrate for at least 30 min. The preparation was then incubated with the voltage-sensitive dye RH-237 (15 μM; Biotium) for 15 min. After the dye incubation period, superfusion was resumed with blebbistatin (10 μM; Cayman Chemical Company) added to the superfusate to suppress contractile activity and prevent motion artifacts. Experiments were performed in sinus rhythm so that the cycle length (i.e. beating rate) of the atrial preparation was free to change. RH-237-loaded atrial preparations were illuminated with light from the X-Cite Xylis Broad Spectrum LED Illumination System (Excelitas Technologies) and filtered with a 520/35 nm excitation filter (Semrock). Emitted fluorescence was separated by a dichroic mirror (560 nm cut-off; Semrock) and filtered by a 715 nm long-pass emissions filter (Andover Corp.). Recordings were captured using a high-speed CMOS camera (MiCAM03-N256, SciMedia). We mapped conduction in the region of the right atrial posterior wall around the point of initial electrical excitation, which corresponds to the activation of the SAN. The region that was

mapped extended from the superior vena cava to the inferior cava along the edge of the crista terminalis, based on the known anatomical location of the SAN in the mouse heart[5,6,9]. Data were captured from an optical field of view of 6.8 x 6.8 mm at a frame rate of 1000 frames/s using BrainVision software (BrainVision Inc.). The spatial resolution was 26.6 x 26.6 μM for each pixel. Magnification was constant in all experiments and no pixel binning was used. All optical data were analyzed using custom software written in MATLAB® (Mathworks) as we have previously described.[3-5]

Patch clamping in sinoatrial node myocytes

The procedures for isolating single pacemaker myocytes from the sinoatrial node (SAN), of the mouse have been described previously[5,8] and were as follows. Mice were administered a 0.2 ml intraperitoneal injection of heparin (1000 IU/ml) to prevent blood clotting. Following this, mice were anesthetized by isoflurane inhalation and then euthanized by cervical dislocation. The heart was excised into Tyrode's solution (35ºC) consisting of (in mmol/L) 140 NaCl, 5.4 KCl, 1.2 KH_2PO4, 1.0 $MgCl_2$, 1.8 $CaCl_2$, 5.55 glucose, and 5 HEPES, with pH adjusted to 7.4 with NaOH. The sinoatrial node (SAN) region of the heart was isolated by separating the atria from the ventricles, cutting open the superior and inferior venae cavae, and pinning the tissue so that the crista terminalis could be identified. The SAN area is located in the intercaval region adjacent to the crista terminalis. This SAN region was cut into strips, which were transferred and rinsed in a 'low Ca^{2+}, Mg^{2+} free' solution containing (in mmol/L) 140 NaCl, 5.4 KCl, 1.2 KH_2PO_4, 0.2 $CaCl_2$, 50 taurine, 18.5 glucose, 5 HEPES and 1 mg/ml bovine serum albumin (BSA), with pH adjusted to 6.9 with NaOH. SAN tissue strips were digested in 5 ml of 'low Ca^{2+}, Mg^{2+} free' solution containing collagenase (type II, Worthington Biochemical 4 Corporation), elastase (Worthington Biochemical Corporation) and protease (type XIV, Sigma Chemical Company) for 30 min. Then the tissue was transferred to 5 ml of modified KB solution containing (in mmol/L) 100 potassium glutamate, 10 potassium aspartate, 25 KCl, 10 KH_2PO_4, 2 $MgSO_4$, 20 taurine, 5

creatine, 0.5 EGTA, 20 glucose, 5 HEPES, and 0.1% BSA, with pH adjusted to 7.2 with KOH. The tissue was mechanically agitated using a wide-bore pipette. This procedure yielded individual SAN myocytes with cellular automaticity that was recovered after readapting the cells to a physiological concentration of Ca^{2+}. SAN myocytes were identified by their small spindle shape and ability to beat spontaneously in the recording chamber when superfused with normal Tyrode's solution. When patch-clamped, SAN myocytes displayed spontaneous action potentials and the hyperpolarization-activated current, I_f. The capacitance of single SAN myocytes was 20–35 pF.

Spontaneous action potentials (APs) and stimulated APs were recorded using the perforated patch-clamp technique on single SAN, with the exception of the 8-Br-cAMP studies in which the whole cell configuration of the patch-clamp technique was used. This was so that 8-Br-cAMP (10 μM), which was included in the pipette solution, could enter the myocytes from the recording pipette. I_f, L-type Ca^{2+} currents ($I_{Ca,L}$) and Na+ current (I_{Na}) were recorded by voltage clamping single SAN using the patch-clamp technique in the whole cell configuration. APs and membrane currents were recorded at room temperature (22-23℃). For recording APs and I_f the recording chamber was superfused with a normal Tyrode's solution (22 – 23ºC) containing (in mmol/L) 140 NaCl, 5 KCl, 1 $MgCl_2$, 1 $CaCl_2$, 10 HEPES, and 5 glucose, with pH adjusted to 7.4 with NaOH. The pipette filling solution for APs and I_f contained (in mmol/L) 135 KCl, 0.1 $CaCl_2$, 1 $MgCl_2$, 5 NaCl, 10 EGTA, 4 Mg-ATP, 6.6 Na-phosphocreatine, 0.3 Na-GTP and 10 HEPES, with pH adjusted to 7.2 with KOH. Amphotericin B (200 μg/ml) was added to this pipette solution to record APs with the perforated patch clamp technique. $BaCl_2$ (1×10^{-4} mol/L) was added to the superfusate when recording I_f, in order to eliminate any inward rectifier K^+ current that could be present at low levels in some SAN myocytes. For recording $I_{Ca,L}$ SAN myocytes were superfused with a modified Tyrode's solution (22 – 23℃) containing the following (in mmol/L) 140 TEA-Cl, 5.4 CsCl, 2 $CaCl_2$, 1 $MgCl_2$, 10 HEPES, and 5 glucose with pH adjusted to 7.4 with CsOH. The pipette solution for $I_{Ca,L}$ contained (in mmol/L) 135 CsCl, 0.2 $CaCl_2$, 1 $MgCl_2$, 5 NaCl,

5 EGTA, 4 Mg-ATP, 6.6 Naphosphocreatine, 0.3 Na-GTP and 10 HEPES, with pH adjusted to 7.2 with CsOH. For recording I_{Na} atrial myocytes were superfused with a modified Tyrode's solution (22 – 23°C) containing the following (in mM): 130 CsCl, 5 NaCl, 5.4 TEA-Cl, 1 $MgCl_2$, 1 $CaCl_2$, 10 HEPES, 5.5 glucose, (pH 7.4, adjusted with CsOH). Nitrendipine (10 μM) was added to the superfusate to block $I_{Ca,L}$. The pipette solution for I_{Na} contained (in mM): 120 CsCl, 5 NaCl, 1 $MgCl_2$, 0.2 $CaCl_2$, 10 HEPES, 5 MgATP, 0.3 Na-GTP, 5 BAPTA (pH 7.2, adjusted with CsOH).8-Br-cGMP (10μM; Sigma) was dissolved in the pipette solution so that it could be applied intracellularly under whole-cell recording conditions. Cells were dialyzed for a minimum of 8 min to allow the effects of 8-Br-cGMP to reach maximum levels. Control recordings were measured 30 s after membrane rupture, before the compounds had begun to elicit their effects.

Micropipettes were pulled from borosilicate glass (with filament, 1.5 mm OD, 0.75 mm ID, Sutter Instrument Company) using a Flaming/Brown pipette puller (model p-87, Sutter Instrument Company). The resistance of these pipettes was 4–8MΩ when filled with recording solution. Micropipettes were positioned with a micromanipulator (Burleigh PCS-5000 system) mounted on the stage of an inverted microscope (Olympus IX71). Seal resistance was 2–15 GΩ. Rupturing the sarcolemma in the patch for voltage clamp experiments resulted in access resistances of 5–15MΩ. Series resistance compensation averaged 80–85% using an Axopatch 200B amplifier (Molecular Devices). For perforated patch clamp experiments, access resistance was monitored for the development of capacitative transients upon sealing to the cell membrane with Amphotericin B in the pipette. Typically, access resistance became less than 30MΩ within 5min of sealing onto the cell, which was sufficient for recording spontaneous APs in current clamp mode. Data were digitized using a Digidata 1440 and pCLAMP 10 software (Molecular Devices) and stored on computer for post hoc analysis. Spontaneous AP parameters, including the maximum diastolic potential (MDP), the slope of the diastolic depolarization (DD slope), the maximum AP upstroke velocity (V_{max}), the AP overshoot and the AP duration at 50% repolarization (APD_{50}) were analyzed. The DD slope was measured by fitting a straight line to

the linear portion of this AP component. Activation kinetics for I_f were determined by normalizing tail currents at each voltage to the maximum current level at -130 mV and fitting the data to the Boltzmann function: I/Imax=1/(1+exp[(Vm-V1/2)/k]) where V_m is the potential of the voltage clamp step, V1/2 is the voltage at which 50% activation occurs and k is the slope factor. I_f time constants of activation were measured by fitting a monoexponential equation to I_f raw recordings. $I_{Ca,L}$ and I_{Na} activation kinetics were determined by calculating chord conductance (G) with the equation $G=I/(V_m-E_{rev})$, where V_m represents the depolarizing voltages and E_{rev} is the reversal potential estimated from the current-voltage relation of $I_{Ca,L}$. Maximum conductance (G_{max}) and $V_{1/2}$ of activation for $I_{Ca,L}$ and I_{Na} were determined using the following function: $G=[(V_m-V_{rev})][G_{max}][-1/[(1+\exp((V_m-V_{1/2})/k))+1]]$

cAMP Assay

cAMP levels were measured from live cells as we have reported previously[10]. Two mouse SAN myocyte isolations were performed as described above, pooled together to ensure adequate cell number, and centrifuged (2000 rpm) for 10 minutes. The supernatant was removed, and the pellet was resuspended in normal Tyrode's solution. A hemocytometer was used to determine myocyte density. Cells were incubated with either Tyrode's solution (untreated control), CNP (100 nM), or the PDE3 inhibitor milrinone (10 μM) for 15 min at room temperature (21°C). Intracellular cAMP concentrations were then determined using a HTRF cAMP Femto2 kit (Cisbio US, kit #62AM4PEB) according to the manufacturer's instructions and normalized to myocyte density.

Atrial and ventricular cAMP levels were assessed using Cyclic AMP Competitive ELISA Kit (Catalog # EMSCAMPL). Tissue was frozen in liquid nitrogen, ground to a fine powder and homogenized in 10 volumes of 0.1 M HCl. The sample was centrifuges at 1500G for 10 minutes. Supernatants were transferred to clean test tubes and protein concentration was

determined with a Bradford assay. Tissue cAMP concentrations were then determined using the above kit according to manufactures instructions and normalized to protein concentration.

cGMP and CNP assays

Whole atrial preparations containing the SAN were snap frozen in liquid nitrogen in order to ensure enough tissue cGMP for assay detection. Frozen atria were homogenized on ice in 5% trichloroacetic acid (TCA) and centrifuged at 1500g for 10 minutes. Supernatants were transferred to clean test tubes and the TCA was extracted using water-saturated ether. The pellet was re-suspended in ice-cold RIPA buffer and protein concentration was quantified using a Bio-Rad DC™ Protein Assay Kit II (Bio-Rad). Tissue cGMP concentration was then determined using a cGMP ELISA kit (Cayman Chemical, kit #581021) according to the manufacturer's instructions and normalized to protein concentration.

cGMP and CNP were also measured in in the plasma using commercially available kits according the manufacturer's instructions. For these studies, blood was collected by cardiac puncture, placed in collection tubes containing heparin and EDTA (ED Biosciences) and centrifuged at 2000 RPM for 15 min. Plasma was removed and subsequently used for cGMP and CNP assays.

Phosphodiesterase activity assay

Two SAN samples were pooled together and homogenized in non-denaturing lysis buffer (20 mM Tris HCl, 137 mM NaCl, 1% Nonident P-40, 2 mM EDTA) and Protease Inhibitor Cocktail (Sigma-Aldrich) to ensure adequate protein concentration. Tissue homogenates were then desalted using Zeba Spin Desalting Columns (Thermofisher Scientific). Protein concentration was measured as described above. Phosphodiesterase activity was then measured using the Phosphodiesterase Activity Assay Kit (Abcam, kit#ab13946) as per the manufacturer's instructions. The activities of PDE2, PDE3 and PDE4 were quantified as the

difference between the baseline 5'-AMP (pmol) produced after 60 minutes and the amount produced in the presence of either EHNA (10 μM; PDE2 inhibitor), milrinone (10 μM; PDE3 inhibitor), or rolipram (10 μM; PDE4 inhibitor). Final activity was standardized to sample protein concentration and represented as 5'-AMP (pmol/mg protein/min).

Quantitative polymerase chain reaction

Quantitative gene expression in the SAN was performed as we described previously[5,11]. Intron spanning primers (Integrated DNA Technologies) were designed for *Npr1* (NPR-A), *Npr2* (NPR-B), *Npr3* (NPR-C), *Hcn1*, *Hcn2*, *Hcn4*, *Cacna1a* ($Ca_V1.2$), *Cacna1d* ($Ca_V1.3$), *Gja5* (Cx40), *Gja1* (Cx43), *Gjc1* (Cx45), *pde2a* (PDE2A), *pde3a* (PDE3A), *pde4a* (PDE4A), *pde4b* (PDE4B), and *pde4d* (PDE4D). GAPDH was used as the reference gene. Primer sequences are provided Table S4. Following synthesis, primers were reconstituted in nuclease free water at a concentration of 100 μM and stored at -20°C. All primer sets were validated in order to determine optimal annealing temperature as well as confirmation of ideal amplification efficiency (between 90-110% copy efficiency per cycle). RNA was extracted in PureZOL™ RNA isolation reagent according to kit instructions (Aurum Total RNA Fatty and Fibrous Tissue Kit, Bio-Rad). RNA was eluted in 40 μl of elution buffer from the spin column. RNA purity and quantity were determined using a NanoDrop ND-1000 spectrophotometer (NanoDrop Technologies, Wilmington, DE, USA). First strand synthesis reactions were performed using the iScript cDNA synthesis kit (Bio-Rad) according to kit instructions. Lack of genomic DNA contamination was verified by reverse transcription (RT)-PCR using a no RT control. RT-qPCR using BRYT green dye (Promega) was used to assess gene expression.

Western blotting

Protein samples were extracted from two SANs and pooled for each experimental replicate in order to ensure sufficient protein[5]. Tissues were pre-cooled in liquid nitrogen and homogenized in an ice-cold RIPA buffer (50 mM Tris, 150 mM NaCl, 1 mM EDTA, 25 mM sucrose, 1% Triton, 0.1% SDS) containing 0.5 mM DTT (1,4-Dithiothreitol, Roche) and Protease Inhibitor Cocktail (SigmaAldrich). Preparation was centrifuged at 10000rpm at 4ºC for 10mins. Protein concentrations were measured as described above. Protein samples (25 µg/lane) were separated by 12% SDS-polyacrylamide gels (SDS-PAGE) and transferred onto Biotrace™ NT nitrocellulose Transfer Membrane (VWR). The membrane was blocked with 1% casein in tris-buffered saline (TBS; Bio-Rad) for 1 hour and incubated overnight at 4ºC with rabbit primary antibodies. Primary antibodies used, concentrations, and suppliers can be found in the Major Resources Table. The membrane was washed 3 times with TBST (TBS with 1% Tween 20 (Bio-Rad)) and incubated with goat anti-rabbit IgG coupled to horseradish peroxidase (HRP; Abcam) at 1:20000 for 1 hour at room temperature. Then the membrane was washed again 3 times with TBST. ECL (Bio-Rad) was added, incubated for 5 min and the membrane was scanned using the ChemiDoc system (Bio-Rad). We quantified expression of each of these proteins based on the identification of bands at the predicted molecular according to the information from the supplier.

Histology and immunohistochemistry

Interstitial fibrosis in the SAN was assessed using picrosirius red (collagen) and fast green (myocardium) staining of paraffin embedded sections (8 µM) through the SAN cut perpendicular to the crista terminalis. Adjacent sections were used for immunostaining of HCN4 in order to confirm the SAN region as we have described previously.[5,12] For the immunohistochemistry, sections were deparaffinised and blocked for 1 hr with 15% goat serum (Gibco). Sections were then incubated with anti-HCN4 primary antibody (Alomone Labs) at a dilution of 1:100 overnight in a light –protected chamber. Sections were then incubated with

Alexa Fluor 488 Goat anti-Rabbit IgG (H+L; Invitrogen) secondary antibody at a dilution of 1:100 for 1 hr at room temperature. Sections were mounted with ProLong Gold Antifade Mountant (Invitrogen) and imaged by confocal microscopy at 488/519 nm (Zeiss LSM 5 Exciter).

Picrosirius red staining was also used to assess right atrial and left ventricular fibrosis using paraffin embedded section (5 µM) through these tissue regions. Fibrosis in all regions was quantified using ImageJ software.

Supplemental Figures

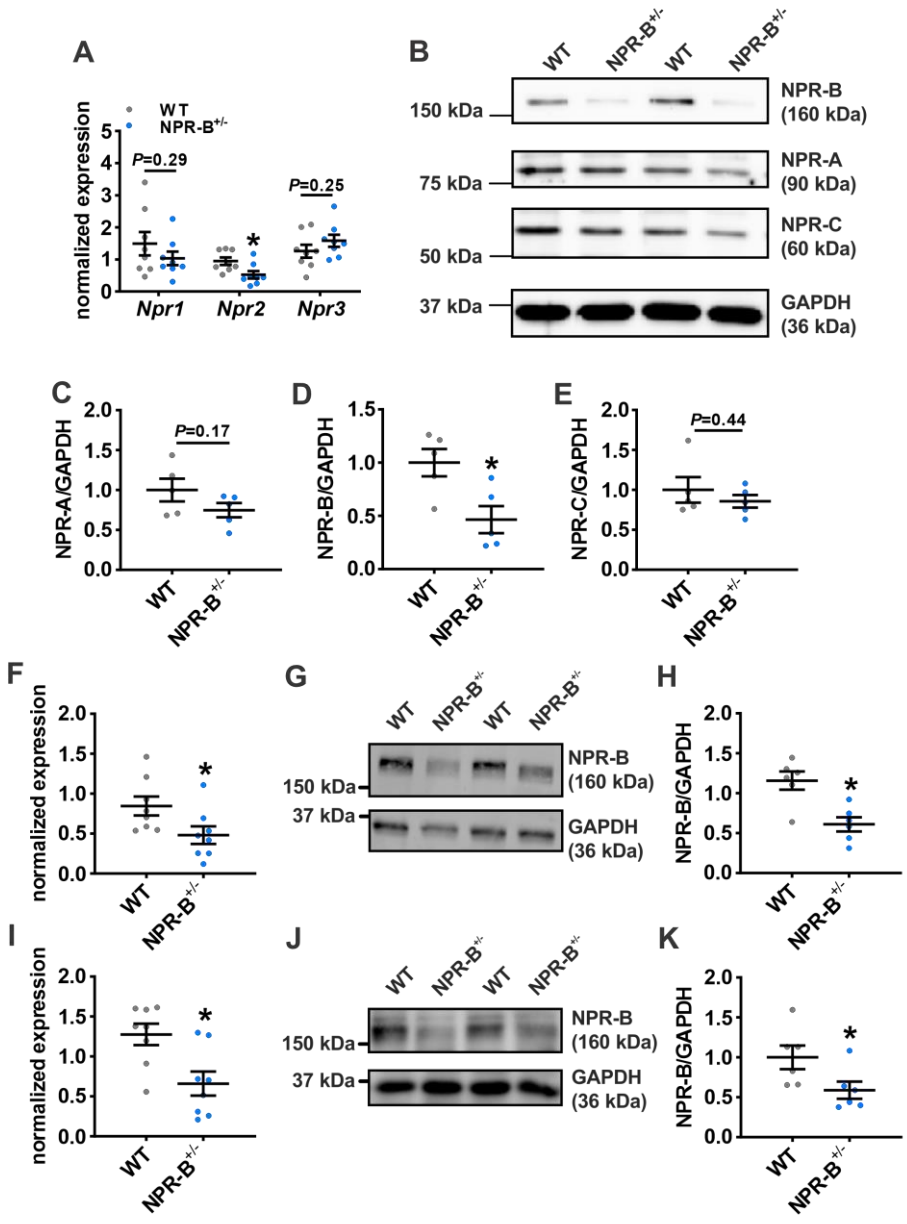

Figure S1: Expression of natriuretic peptide receptors (NPRs) in the SAN, atrium and ventricle in NPR-B$^{+/-}$ mice. **A,** mRNA expression of *Npr1* (encodes NPR-A), *Npr2* (encodes NPR-B) and *Npr3* (encodes NPR-C) in the SAN of WT (n=8) and NPR-B$^{+/-}$ (n=8) mice. *P<0.05 vs WT by Student's t-test. **B,** Representative Western blots for NPR-A, NPR-B and NPR-C protein expression in the SAN of WT and NPR-B$^{+/-}$ mice. Molecular weight markers are indicated on the left side of the blot. **C-E,** Summary of protein expression of NPR-A (**C**), NPR-B (**D**) and NPR-C (**E**) in the SAN of WT (n=5) and NPR-B$^{+/-}$ (n=5) mice. *P<0.05 vs WT by Student's t-test. **F,** mRNA expression on *Npr2* in the right atrium of WT (n=8) and NPR-B$^{+/-}$ (n=8) mice. P<0.05 vs. WT by Student's t-test **G and H,** Representative Western blot (**G**) and summary of NPR-B

protein expression (**H**) in the right atrium of WT (*n*=6) and NPR-B$^{+/-}$ (*n*=6) mice. **I,** mRNA expression on *Npr2* in the left ventricle of WT (*n*=8) and NPR-B$^{+/-}$ (*n*=8) mice. *P*<0.05 vs. WT by Student's *t*-test **J and K,** Representative Western blot (**J**) and summary of NPR-B protein expression (**K**) in the left ventricle of WT (*n*=6) and NPR-B$^{+/-}$ (*n*=6) mice.

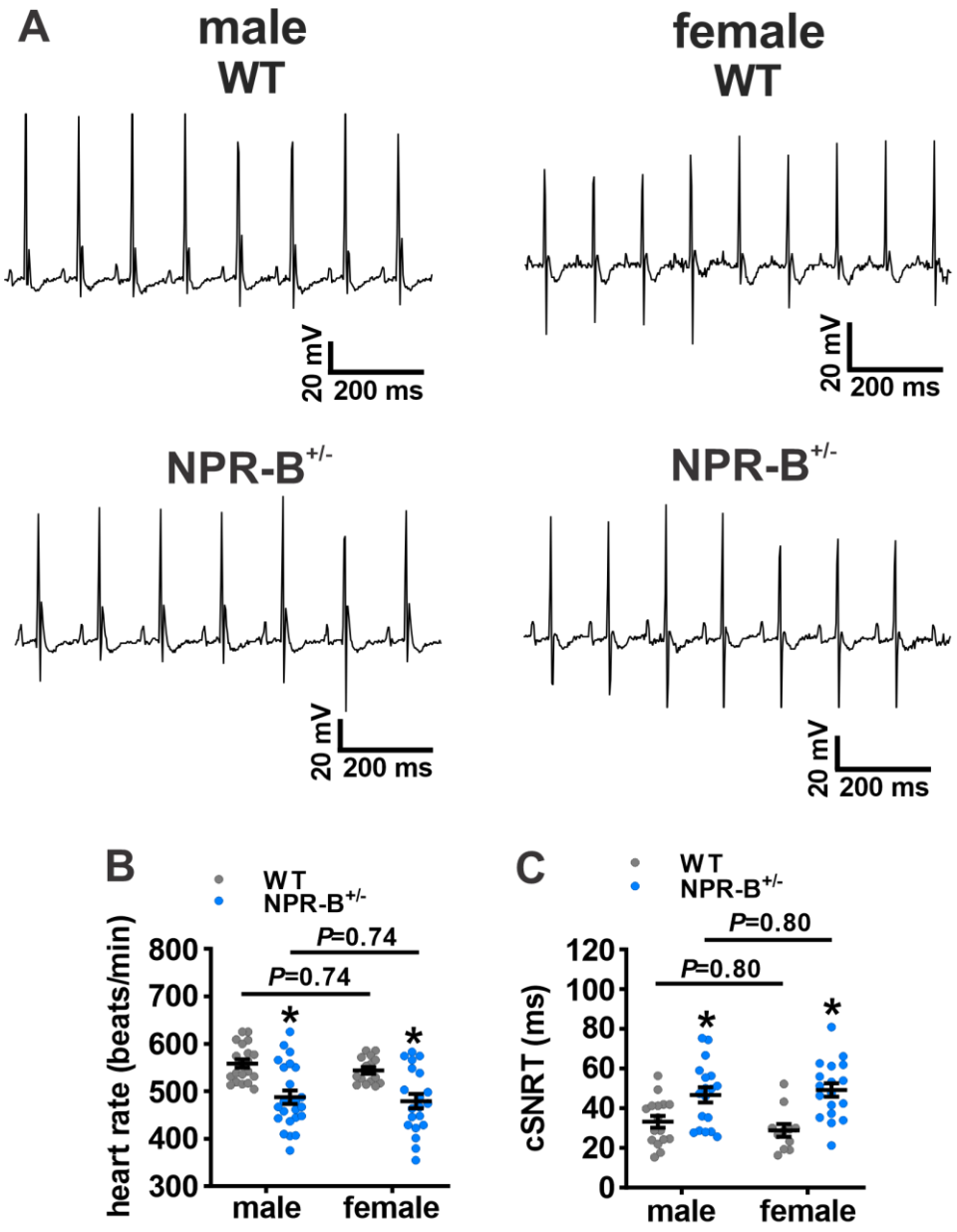

Figure S2: Heart rate and cSNRT in male and female NPR-B$^{+/-}$ mice. **A,** Representative ECG recordings from anesthetized male and female WT and NPR-B$^{+/-}$ mice. **B**, Summary of heart rate in WT male (*n*=20), WT female (*n*=15), NPR-B$^{+/-}$ male (*n*=23) and NPR-B$^{+/-}$ female (*n*=20) mice. **C,** Summary of cSNRT in WT male (*n*=16), WT female (*n*=11), NPR-B$^{+/-}$ male (*n*=18) and NPR-B$^{+/-}$ female (*n*=18) mice. **P*<0.05 vs WT by two-way ANOVA with Holm-Sidak posthoc test.

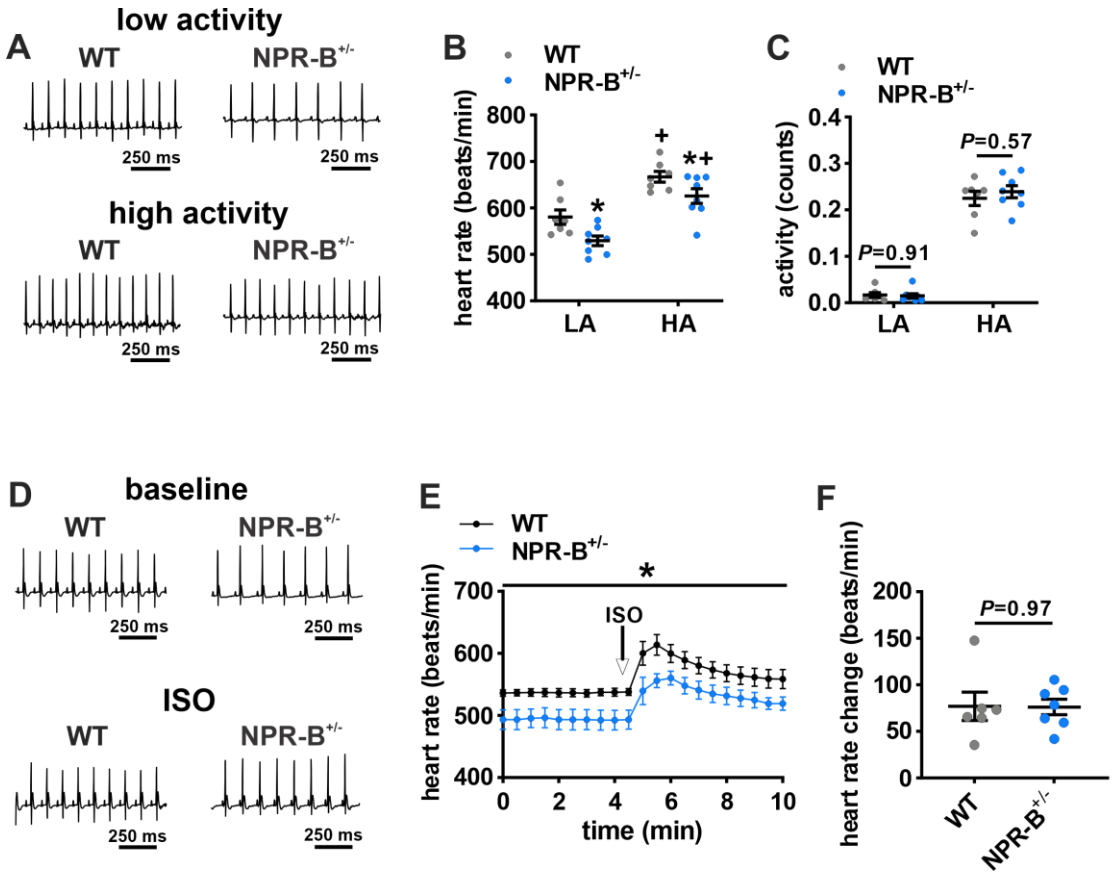

Figure S3: Activity-dependent heart rate and maximum heart rate in NPR-B$^{+/-}$ mice. A, Representative ECGs in WT and NPR-B$^{+/-}$ mice during low activity and high activity. **B,** HR in WT (*n*=7) and NPR-B$^{+/-}$ (*n*=8) mice during low activity (LA) and high activity (HA). **P*<0.05 vs. WT; $^{+}$*P*<0.05 vs LA by two-way ANOVA with Holm-Sidak posthoc test. **C,** Activity during LA and HA in WT (*n*=7) and NPR-B$^{+/-}$ (*n*=8) mice. Data analyzed by two-way ANOVA with Holm-Sidak posthoc test. **D,** Representative ECGs in WT and NPR-B$^{+/-}$ mice at baseline and after subcutaneous injection with isoproterenol (ISO, 100 mg/kg). **E,** HR at baseline and after injection of ISO in WT (*n*=6) and NPR-B$^{+/-}$ (*n*=7) mice. **P*<0.05 vs. WT for main effect of genotype by two-way ANOVA. **F,** Maximum change in HR after ISO injection in WT (*n*=6) and NPR-B$^{+/-}$ (*n*=7) mice. Data analyzed by Student's *t*-test.

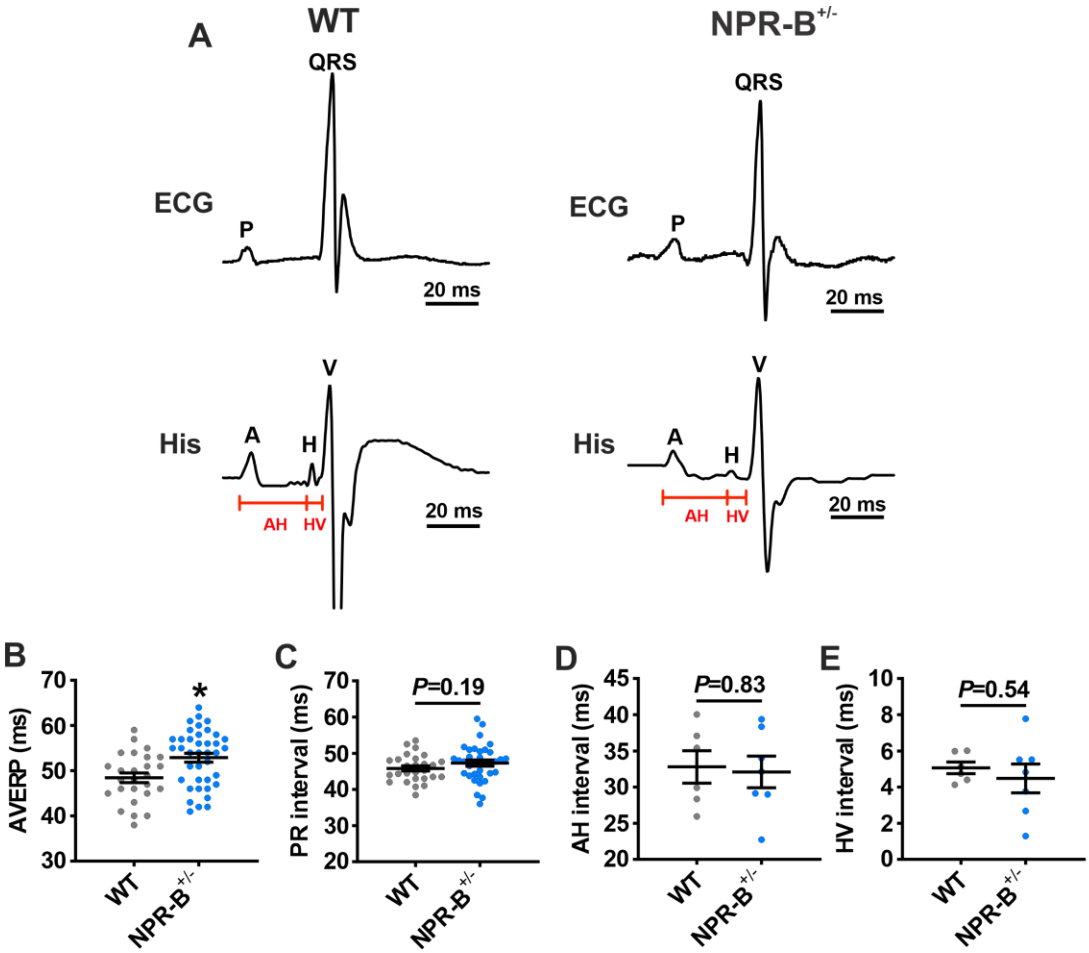

Figure S4: ECG analysis in NPR-B$^{+/-}$ mice. A, Representative surface ECG (top) and intracardiac ECG showing His bundle signal (bottom) in anesthetized WT and NPR-B$^{+/-}$ mice. A, atrial signal; H, His bundle signal; V, ventricular signal. **B,** AV node effective refractory period (AVERP) in WT (*n*=27) and NPR-B$^{+/-}$ (*n*=36) mice. **P*<0.05 vs. WT by Student's *t*-test. **C,** PR interval in WT (*n*=27) and NPR-B$^{+/-}$ (*n*=36) mice. Data analyzed by Student's *t*-test. **D,** AH interval in WT (*n*=6) and NPR-B$^{+/-}$ (*n*=7) mice. Data analyzed by Student's *t*-test. **E,** HV interval in WT (*n*=6) and NPR-B$^{+/-}$ (*n*=7) mice. Data analyzed by Student's *t*-test.

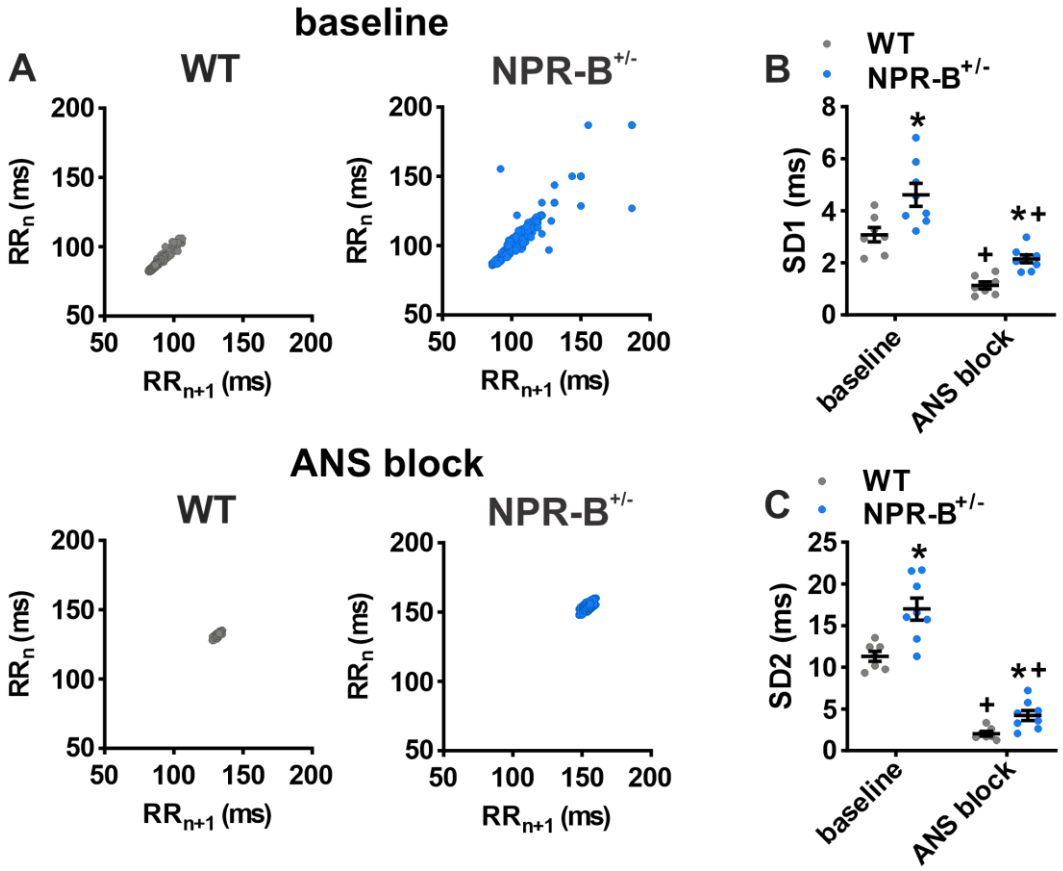

Figure S5: Heart rate variability in NPR-B$^{+/-}$ mice analyzed by non-linear metrics. A, Representative Poincaré plots from telemetric ECG recordings in WT and NPR-B$^{+/-}$ mice in baseline conditions and after autonomic nervous (ANS) system block. **B and C,** SD1 (**B**) and SD2 (**C**) from Poincaré plots in WT (*n*=7) and NPR-B$^{+/-}$ (*n*=8) mice. **P*<0.05 vs. WT; $^{+}$*P*<0.05 vs. baseline by two-way ANOVA with Holk-Sidak posthoc test.

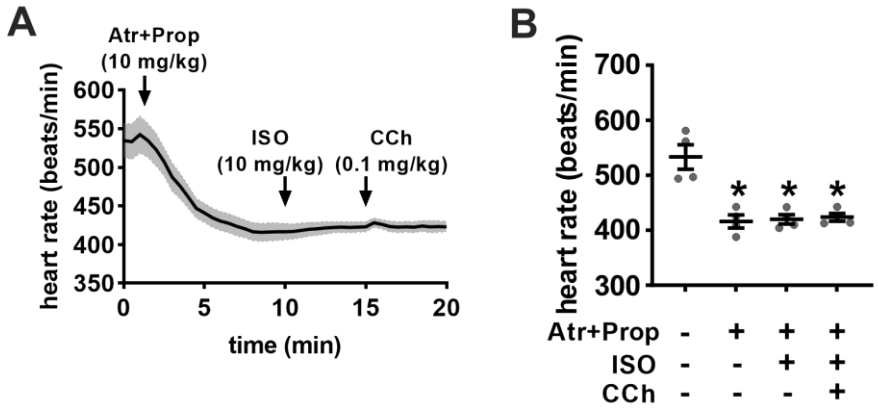

Figure S6: Autonomic nervous system (ANS) blockade induced by injection of atropine and propranolol. A, heart rate was measured continuously. Atropine (Atr) and propranolol (Prop) were given by intraperitoneal injection at doses of 10 mg/kg. After ANS blockade, isoproterenol (ISO, 10 mg/kg) and carbachol (CCh, 0.1 mg/kg) were given 5 min apart. **B,** Heart rate after injection of Atr+Prop, ISO, and CCh. *P<0.05 vs. baseline (i.e. no drugs); n=4 mice. Atr+Prop reduced heart rate. Neither ISO or CCh had any effect on heart rate in the presence of Atr+Prop confirming ANS blockade.

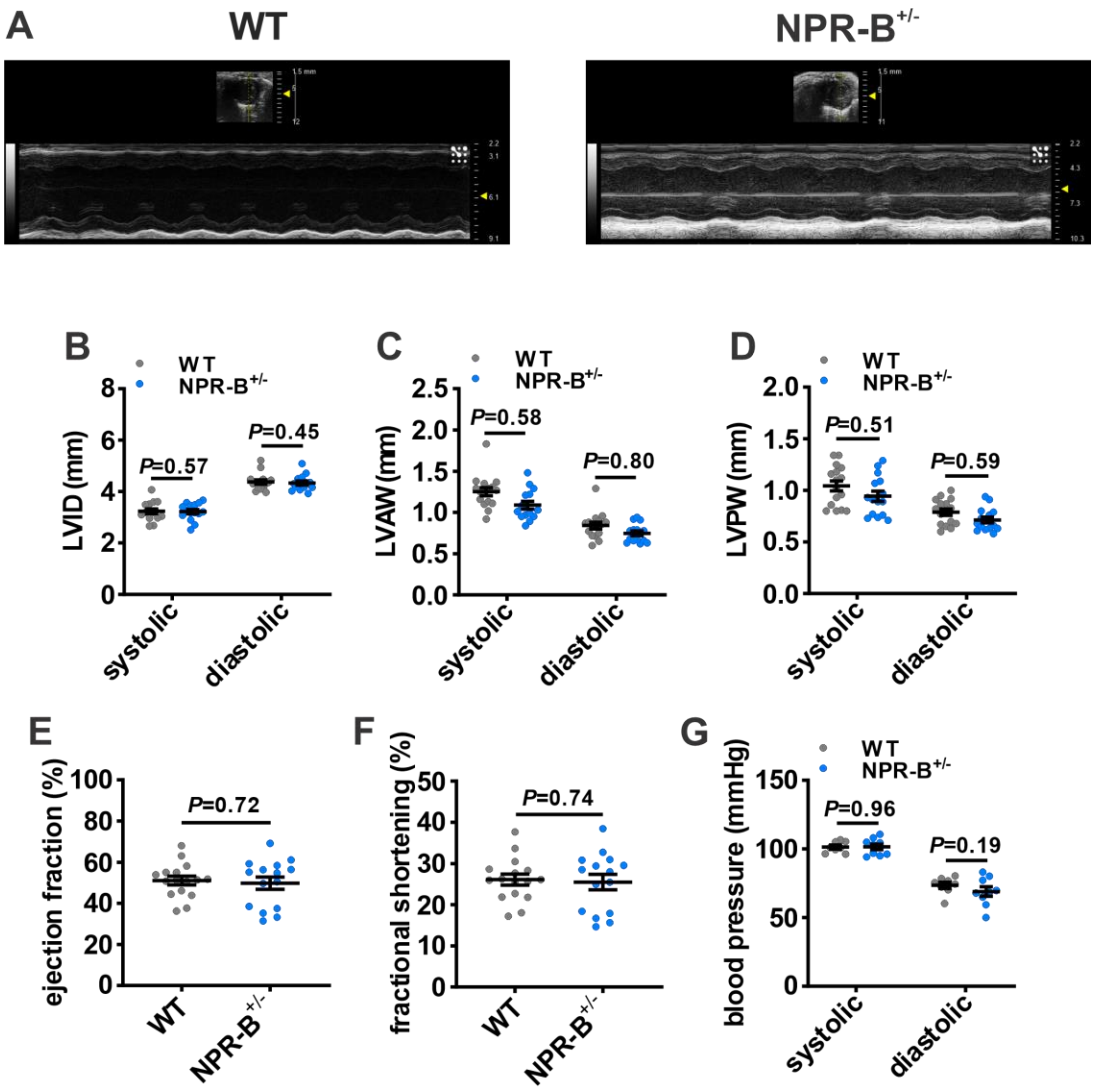

Figure S7: Echocardiography and blood pressure NPR-B$^{+/-}$ mice. **A,** M-mode imaging of the left ventricle from the parasternal short axis view at the midpapillary level in WT and NPR-B$^{+/-}$ mice. Bars on left side of panel represent contrast intensity. Scale bars on right side of panel are measures of distance in mm. **B-D,** Summary data for left ventricular internal diameter (LVID) (**B**), left ventricular anterior wall thickness (LVAW) (**C**), left ventricular posterior wall thickness (LVPW) (**D**) during systole and diastole in WT and NPR-B$^{+/-}$ mice. **E-F,** Summary data for ventricular ejection fraction (**E**) and fractional shortening (**F**) in WT and NPR-B$^{+/-}$ mice. **G,** Systolic and diastolic blood pressure in conscious WT and NPR-B$^{+/-}$ mice. For panels **B-F** *n*=16 WT and 15 NPR-B$^{+/-}$ mice; for panel **G** *n*=8 WT and 9 NPR-B$^{+/-}$ mice. All data analysed by Student's *t*-test.

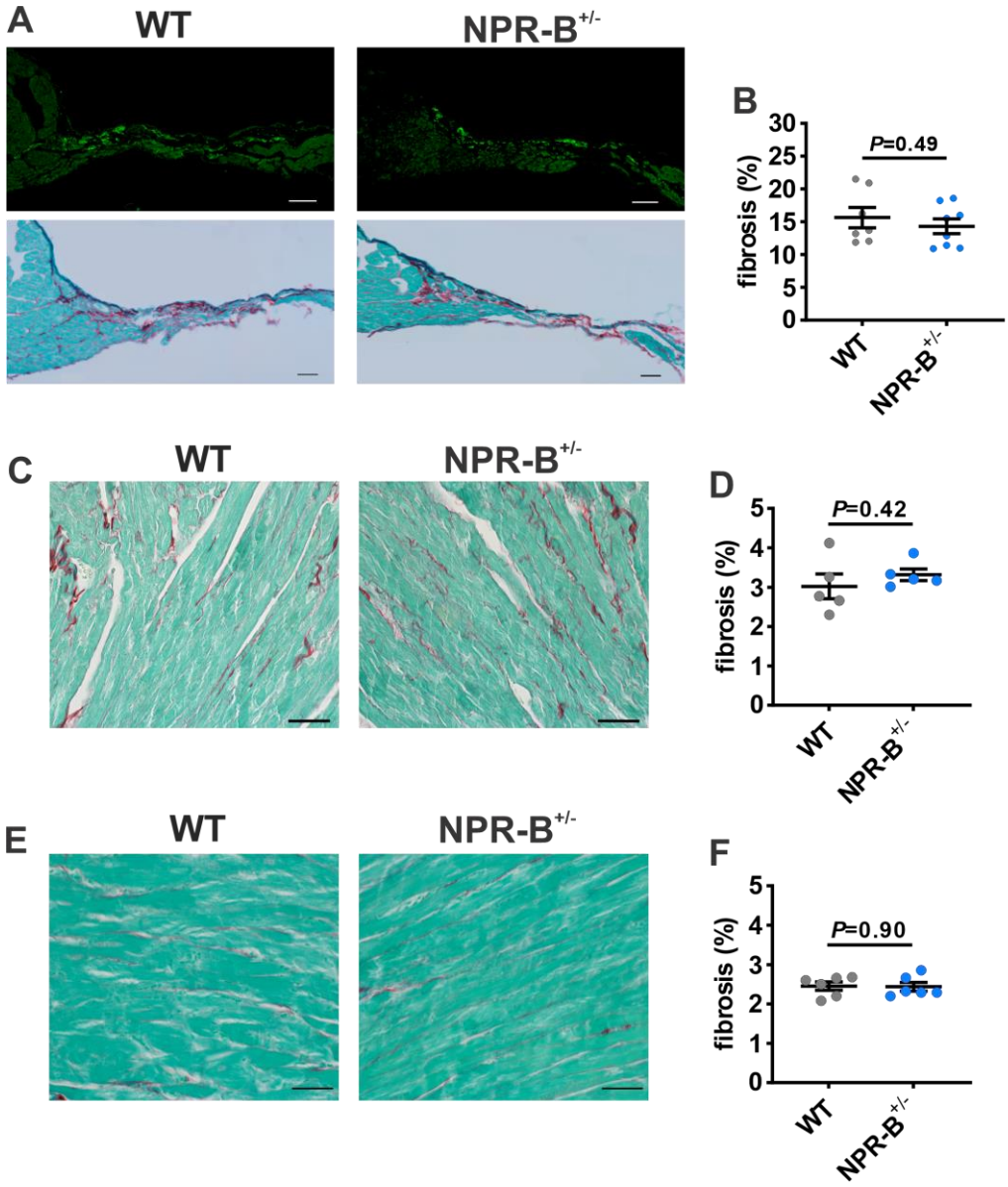

Figure S8: Interstitial fibrosis in NPR-B$^{+/-}$ mice. **A,** Sections through the SAN in WT and NPR-B$^{+/-}$ mice. Top panels illustrate the HCN4-positive zone (green) within the SAN. Bottom panels illustrate the picrosirius red staining from the adjacent section used to identify fibrosis (red). Scale bars = 50 μM. **B,** Summary of SAN fibrosis measured in the HCN4-positive zone of the SAN for WT and NPR-B$^{+/-}$ mice. Data analysed by Student's *t*-test; *n*=7 WT hearts and 8 NPR-B$^{+/-}$ hearts. **C,** Right atrial sections in WT and NPR-B$^{+/-}$ mice. **D,** Summary of right atrial fibrosis in WT and NPR-B$^{+/-}$ mice. Data analyzed by Student's *t*-test; *n*=5 for each genotype. **E,** Left ventricular sections in WT and NPR-B$^{+/-}$ mice. **F,** Summary of left atrial fibrosis in WT and NPR-B$^{+/-}$ mice. Data analyzed by Student's *t*-test; *n*=6 for each genotype.

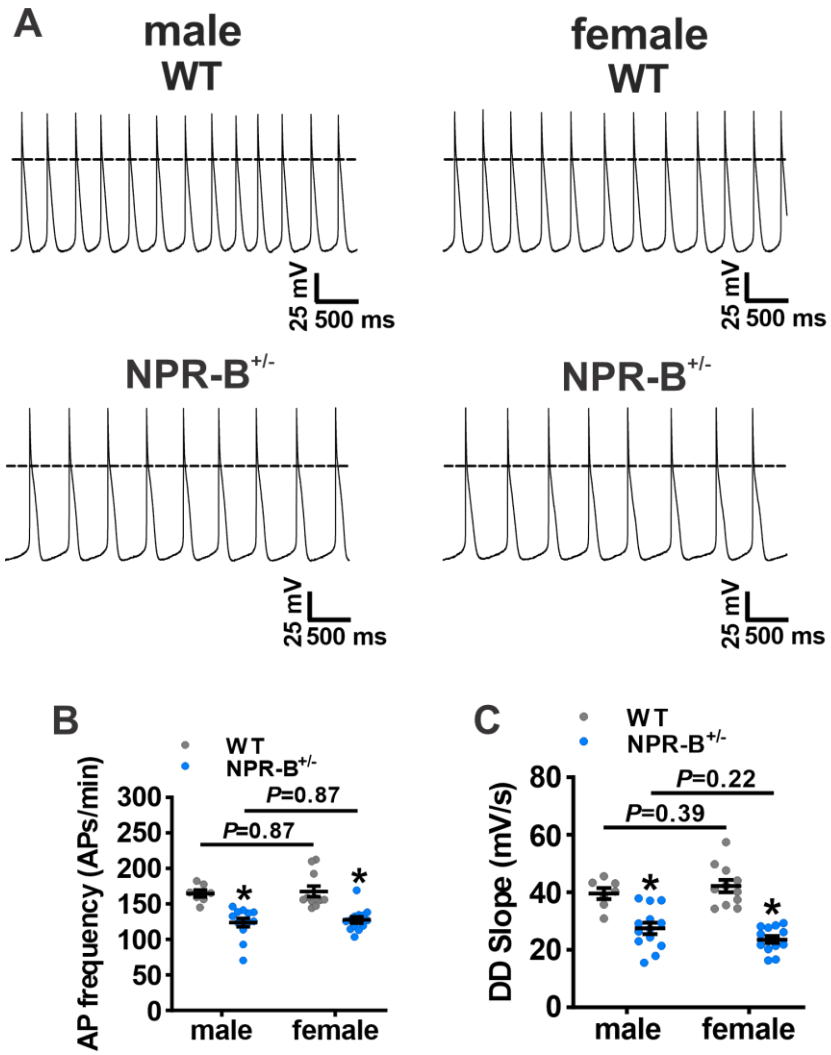

Figure S9: Spontaneous action potential parameters in SAN myocytes from male and female NPR-B$^{+/-}$ mice. **A,** Representative spontaneous AP recordings in isolated SAN myocytes isolated from male and female WT and NPR-B$^{+/-}$ mice. **B-C,** Summary of spontaneous AP frequency (**B**) and DD slope (**C**) in SAN myocytes from male and female WT and NPR-B$^{+/-}$ mice. *n*=7 cells from male WT, 11 cells from female WT, 13 cells from male NPR-B$^{+/-}$, and 13 cells from female NPR-B$^{+/-}$; **P*<0.05 vs WT by two-way ANOVA with Holm-Sidak posthoc test.

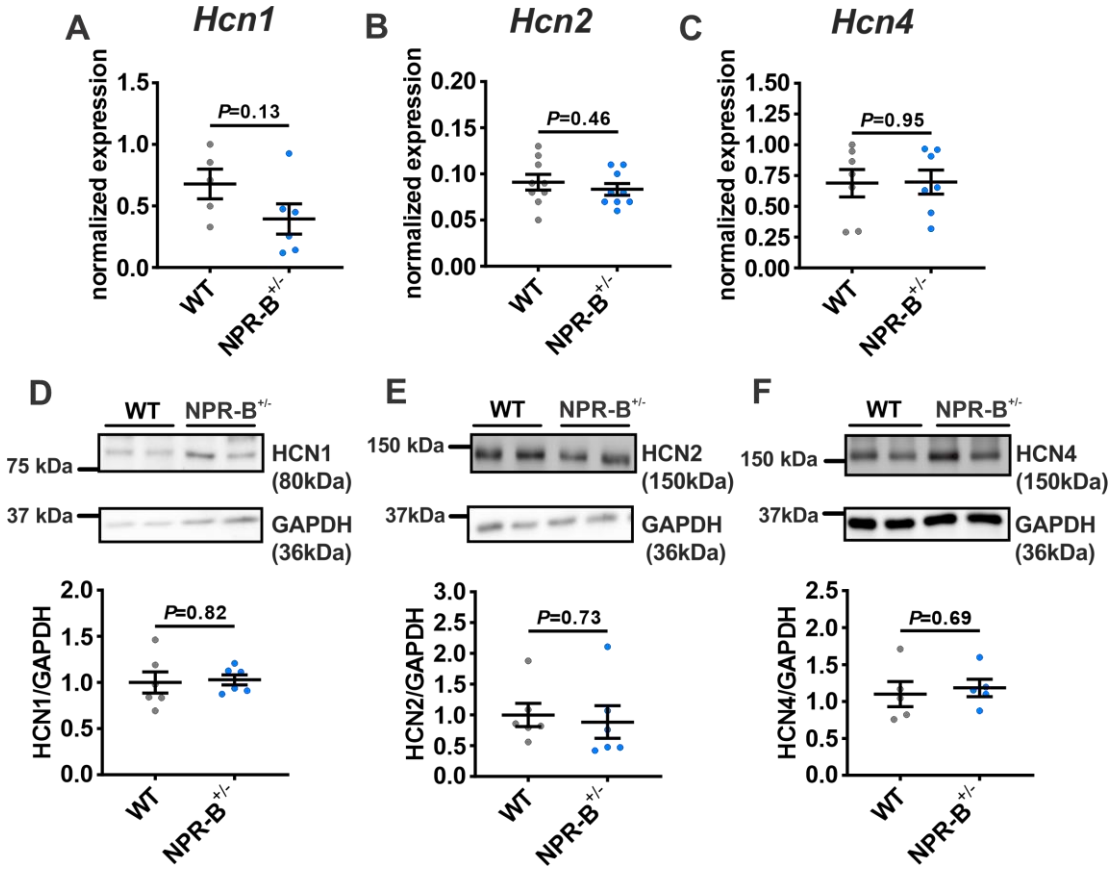

Figure S10: HCN channel expression in the SAN of NPR-B$^{+/-}$ mice. **A-C,** Summary data for mRNA expression of *Hcn1* (*n*=5 WT and 6 NPR-B$^{+/-}$ SANs), *Hcn2* (*n*=9 SAN per genotype), and *Hcn4* (*n*=7 SAN per genotype) in WT and NPR-B$^{+/-}$ mice. Data analysed by Student's *t*-test. **D-F,** Representative Western blots for HCN1, HCN2, and HCN4 proteins in the SAN of WT and NPR-B$^{+/-}$ mice. Molecular weight markers are indicated on the left side of the blot. Summary data for protein expression of HCN1 (*n*=6 SAN per genotype), HCN2 (*n*=6 SAN per genotype), and HCN4 (*n*=5 SAN per genotype) in the SAN of WT and NPR-B$^{+/-}$ mice are shown below each blot. Data analysed by Student's *t*-test.

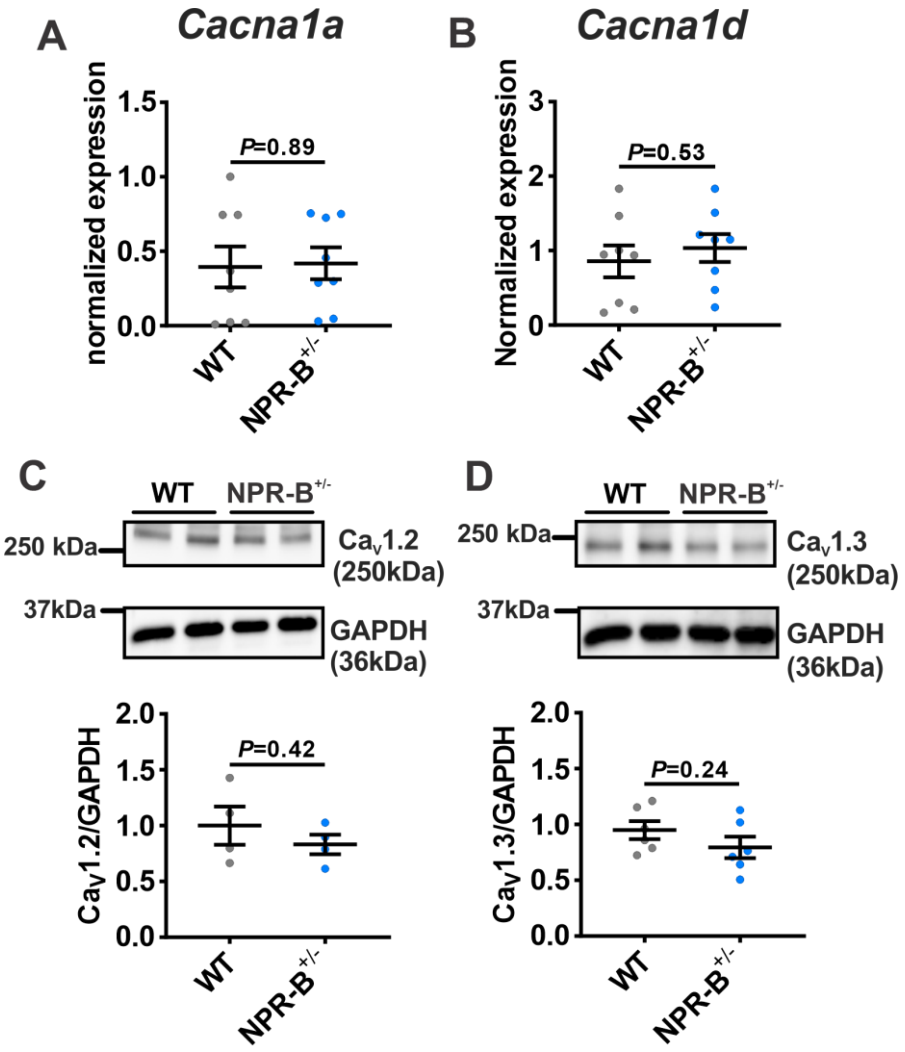

Figure S11: Voltage gated calcium channel expression in the SAN of NPR-B$^{+/-}$ mice. **A-B,** Summary data for mRNA expression of *Cacna1a* (encodes $Ca_V1.2$) and *Cacna1d* (encodes $Ca_V1.3$) in WT (*n*=8 SAN) and NPR-B$^{+/-}$ (*n*=8 SAN) mice. Data analysed by Student's *t*-test. **C-D,** Representative Western blots for $Ca_V1.2$ and $Ca_V1.3$ proteins in the SAN of WT and NPR-B$^{+/-}$ mice. Molecular weight markers are indicated on the left side of the blot. Summary data for protein expression of $Ca_V1.2$ (*n*=4 SAN per genotype) and Ca*V*1.3 (*n*=6 SAN per genotype) in the SAN of WT and NPR-B$^{+/-}$ mice are shown below each blot. Data analysed by Student's *t*-test.

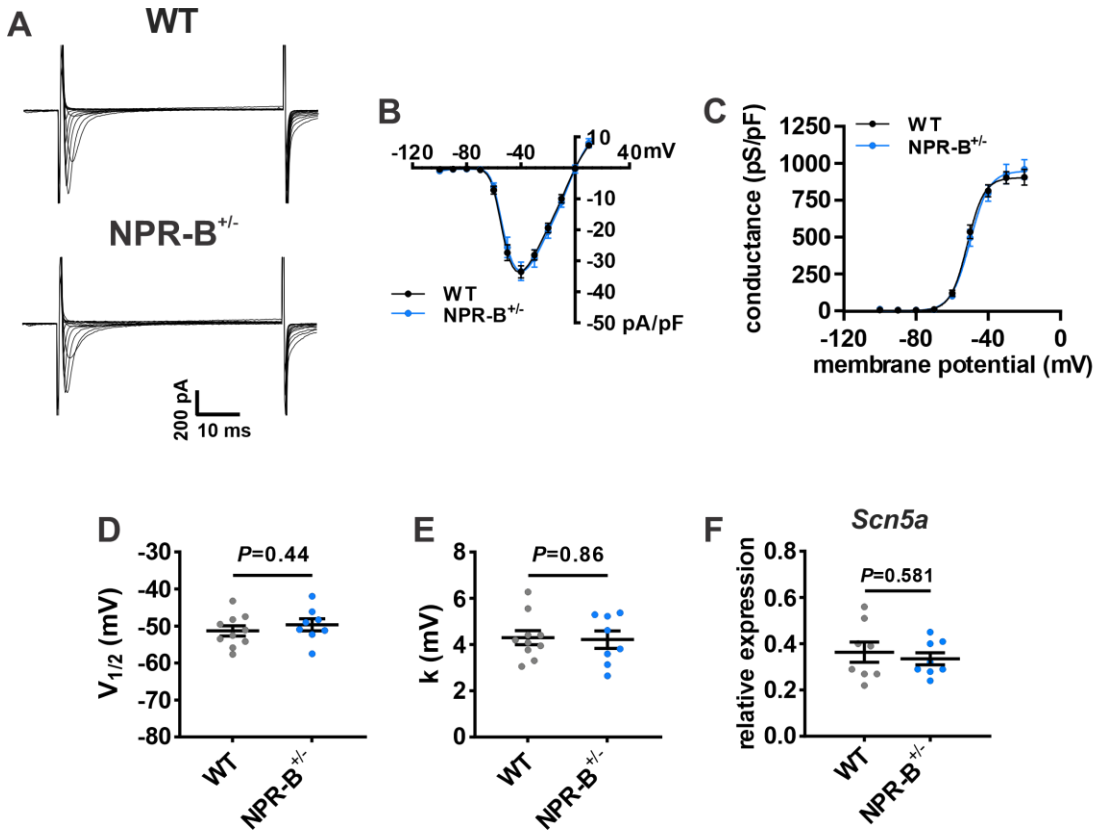

Figure S12: I_{Na} is unaltered in the SAN in NPR-B$^{+/-}$ mice. **A,** Representative I_{Na} recordings in SAN myocytes isolated from WT and NPR-B$^{+/-}$ mice. **B,** Summary I_{Na} IV curves for WT and NPR-B$^{+/-}$ SAN myocytes. **C,** Summary I_{Na} activation curves for WT and NPR-B$^{+/-}$ SAN myocytes. **D-E,** I_{Na} $V_{1/2(act)}$ (**E**) and slope factor (k, **E**) for wildtype and NPR-B$^{+/-}$ SAN myocytes. For panels **B-E**, *n*=10 WT and 8 NPR-B$^{+/-}$ SAN myocytes. Data in panels **B** and **C** analyzed by two-way repeated measures ANOVA with Holm-Sidak posthoc test. Data in panels **D** and **E** analyzed by Student's *t*-test. **F,** mRNA expression of *Scn5a* in WT (*n*=8) and NPR-B$^{+/-}$ (*n*=8) SANs; data analyzed by Student's *t*-test.

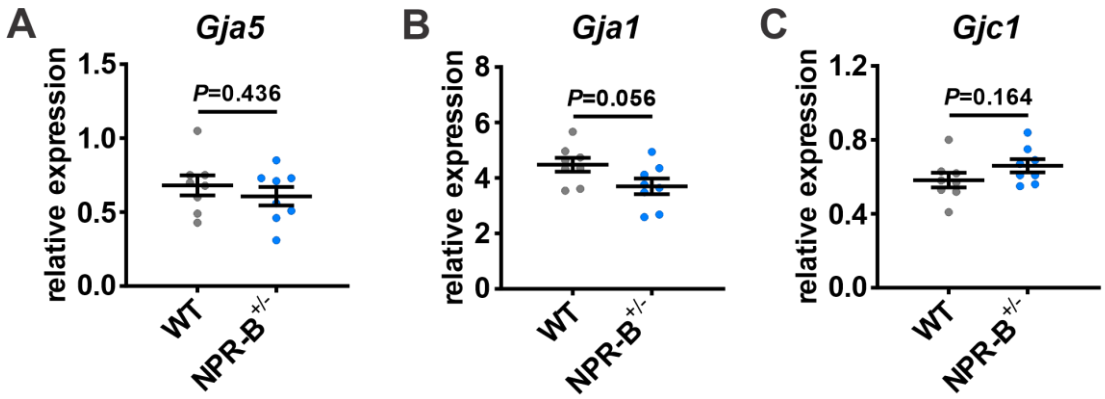

Figure S13: Expression of connexins in the SAN in NPR-B$^{+/-}$ mice. **A-C,** expression of *Gja5* (encodes Cx40, **A**), *Gja1* (encodes Cx43, **B**) and *Gjc1* (encodes Cx45, **C**) in WT (*n*=8) and NPR-B$^{+/-}$ (*n*=8) SANs; data analyzed by Student's *t*-test.

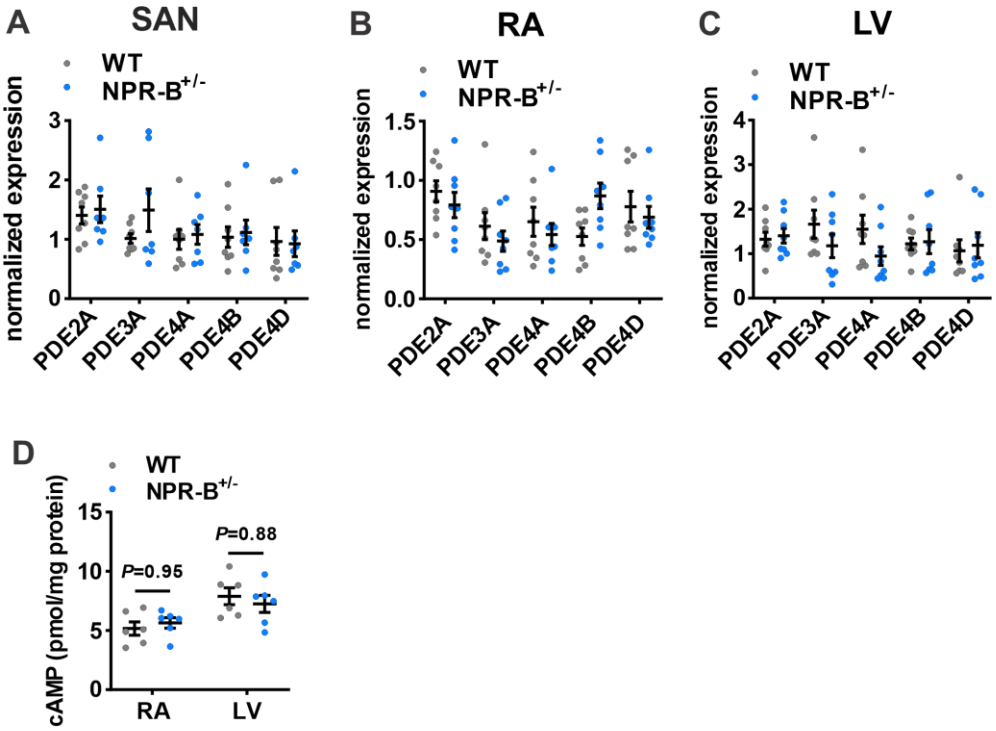

Figure S14: PDE expression and intracellular cAMP levels in the heart in NPR-B$^{+/-}$ mice. **A-C,** mRNA expression of PDEs in the SAN (**A**), right atrium (RA, **B**) and left ventricle (LV, **C**) in WT (*n*=8) and NPR-B$^{+/-}$ (*n*=8) mice. There were no differences between genotypes for the SAN (*P*=0.281), RA (*P*=0.769) or LV (*P*=0.283) by two-way ANOVA with Holm-Sidak posthoc test. **D,** cAMP concentrations in the RA and LV in WT (*n*=6) and NPR-B$^{+/-}$ (*n*=6) mice. Data analyzed by two-way ANOVA with Holm-Sidak posthoc test.

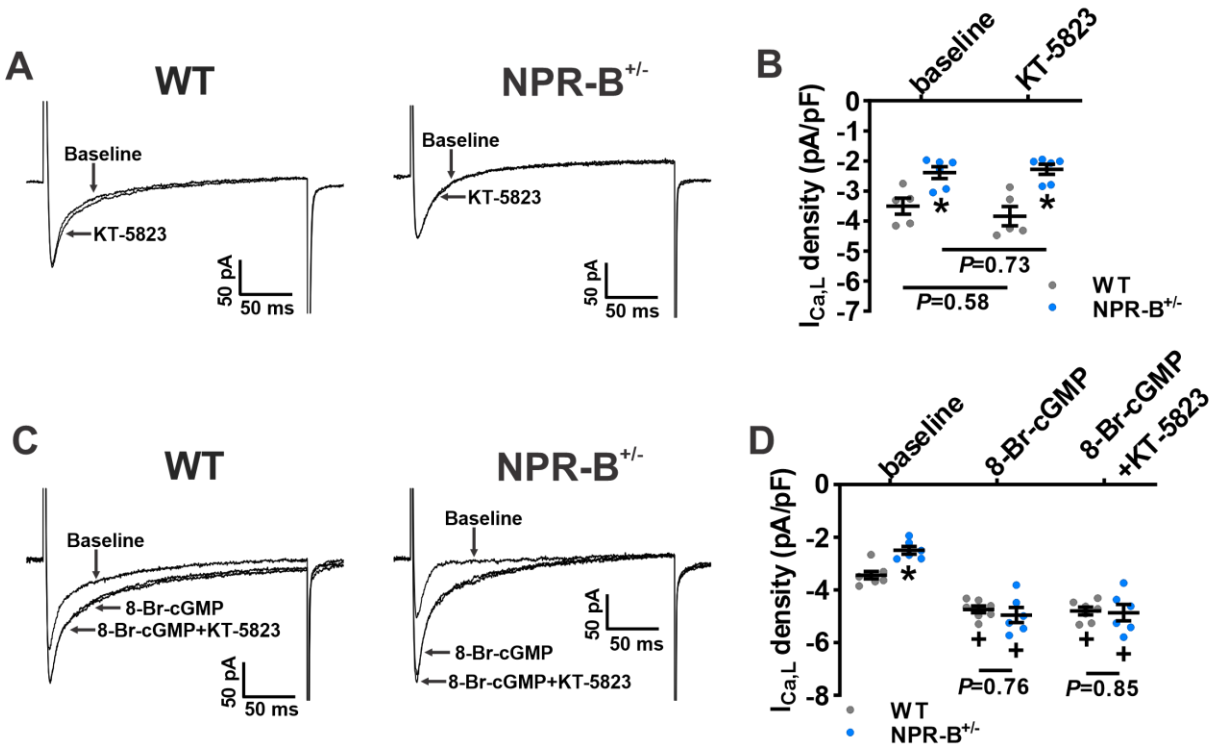

Figure S15: Effect of PKG inhibition on 8-Br-cGMP-stimulated increases in $I_{Ca,L}$ in SAN myocytes from NPR-B$^{+/-}$ mice. A, Representative $I_{Ca,L}$ recordings (measured at -10 mV) at baseline and in the presence of KT-5823 (0.5μM) in isolated SAN myocytes from WT and NPR$^{+/-}$ mice. **B,** Summary of the effects of KT-5823 on $I_{Ca,L}$ in WT (*n*=5 cells from 2 mice) and NPR-B$^{+/-}$ (*n*=6 cells from 2 mice) SAN myocytes. **C,** Representative $I_{Ca,L}$ recordings (measured at -10 mV) at baseline, following intracellular dialysis of 8-Br-cGMP (10μM), and after subsequent application of KT-5823 (0.5μM) in isolated SAN myocytes from WT and NPR-B$^{+/-}$ mice. **D,** Summary of the effects of KT-5823 on the 8-Br-cGMP-stimulated increases in $I_{Ca,L}$ in WT (*n*=7 cells from 2 mice) and NPR-B$^{+/-}$ (*n*=6 cells from 2 mice) SAN myocytes. For panels **B** and **D** **P*<0.05 vs WT within condition; $^{+}$*P*<0.05 vs. baseline within genotype by two-way repeated-measures ANOVA with the Holm-Sidak posthoc test.

Table S1: Action potential parameters in SAN myocytes from wildtype and NPR-B$^{+/-}$ mice.

	WT	**NPR-B$^{+/-}$**	***P* value vs. WT**
n	18	26	
Capacitance (pF)	34.8±1.4	35.8±1.2	0.584
Cycle length (ms)	**364.8±9.4**	**489.4±18.1***	**<0.0001**
AP frequency (APs/min)	**166.6±4.8**	**125.8±3.6***	**<0.0001**
MDP (mV)	-65.6±0.7	-65.5±0.5	0.891
DD Slope (mV/s)	**41.2±1.5**	**25.5±1.2***	**<0.0001**
V_{max} (V/s)	79.7±9.0	69.9±7.8	0.523
OS (mV)	28.5±2.7	26.1±2.4	0.415
APD_{50}	37.0±3.3	39.7±2.5	0.524

n, sample size; MDP, maximum diastolic potential; DD slope, diastolic depolarization slope; Vmax, maximum AP upstroke velocity; OS, overshoot; APD_{50}, AP duration at 50% repolarization; Data are means ± SEM; * *P*<0.05 vs WT by Student's *t*-test.

Table S2: I_f and $I_{Ca,L}$ activation kinetics in wildtype and NPR-$B^{+/-}$ mice.

	WT	**NPR-$B^{+/-}$**	***P* value vs. WT**
	Hyperpolarization Activated "Funny" Current (I_f)		
n	13	15	
$V_{1/2(Act)}$ (mV)	**-110.3±1.4**	**-115.1±1.3***	**0.018**
k (mV)	10.3±0.5	10.1±0.5	0.783
	L-type Ca^{2+} Current ($I_{Ca,L}$)		
n	15	17	
$V_{1/2(Act)}$ (mV)	**-24.3±2.0**	**-17.0±1.6***	**0.008**
Gmax (pS/pF)	**86.2±4.1**	**64.7±3.6***	**<0.001**
k (mV)	7.7±0.3	7.9±0.4	0.750

n, sample size; G_{max}, maximum conductance; $V_{1/2(Act)}$, voltage at which 50% of channels are activated; k, slope factor. **P*<0.05 vs WT by Student's *t*-test.

Table S3: Effect of 8-Br-cGMP on I_f and $I_{Ca,L}$ activation kinetics in wildtype and NPR-$B^{+/-}$ mice.

	WT	NPR-$B^{+/-}$	*P* value vs. WT
Hyperpolarization Activated "Funny" Current (I_f)			
n	10	9	
$V_{1/2(Act)}$ (mV)	-106.3±1.6	-104.3±1.8	0.480
k (mV)	12.3±0.5	13.1±0.7	0.400
L-type Ca^{2+} Current ($I_{Ca,L}$)			
n	10	11	
$V_{1/2(Act)}$ (mV)	-27.2±1.3	-27.2±2.1	0.993
Gmax (pS/pF)	103.8±7.4	95.8±5.3	0.392
k (mV)	7.4±0.7	7.2±0.5	0.858

n, sample size; G_{max}, maximum conductance; $V_{1/2(Act)}$, voltage at which 50% of channels are activated; k, slope factor. **P*<0.05 vs WT by Student's *t*-test.

Table S4: Quantitative PCR primers

Gene of Interest	Forward Primer (5' → 3')	Reverse Primer (3' → 5')	Amplicon Length
Npr1	CGAAGCTTCCAAGGTGTGACAGG	GACACAGCCATCAGCTCCTGGG	152
Npr2	GGGGACTTTCAGCCCGCAGC	GTGGAGTTTTATCACAGGATGGGTCG	150
Npr3	CGAGCGAGTGGTGATCATGTGTG	CTCCACGAGCCATCTCCGTAGG	147
HCN1	CTCTTTTTGCTAACGCCGAT	CATTGAAATTGTCCACCGAA	291
HCN2	CTTCACCAAGATCCTCAGTCTG	GGTCGTAGGTCATGTGGAAA	92
HCN4	CCAGGAGAAGTATAAACAGGTGGAGCG	GTTGATGATCTCCTCTCGAAGTGGCTC	169
CACNA1C	ATGATTCGGGCCTTTGTTCAG	TGGAGTAGGGATGTGCTCG	228
CACNA1D	TGAAGGAGAAGATTGCGCCC	TTGCGGAATGAGTGGCTACG	190
Scn5a	GGAGTACGCCGACAAGATGT	ATCTCGGCAAAGCCTAAGGT	171
Gja5	CACAGTCATCGGCAAGGTCT	ATGGTATCGCACCGGAAGTC	117
Gja1	CCAAGGAGTTCCACCACTTTG	CCATGTCTGGGCACCTCTCT	70
Gjc1	CACTTGGAACACACCCTCTGCTC	GGGAGGTGTTCCTCGTGGCT	159
Pde2a	GGTGGCCTCGAAATCTGTGCTGG	GCATGCGCTGATAGTCCTTCCG	149
Pde3a	GGACAAACCAATTCTTGCTCCAGAACCC	GATACCTGGCTCAGAATACGGCCAC	144
Pde4a	TGGATGCCGTGTTCACAGACCTGG	GTTCTCAAGCACAGACTCATCGTTGTAC	152
Pde4b	CAGGAAAATGGTGATTGACATGGTGTTGG	CGAAGAACCTGTATCCGGTCAGTATAG	152
Pde4d	GGTCATTGACATTGTCCTGGCGACAG	CAGTGCACCATATTCTGAAGGACCTGG	159
GAPDH	AATGGGGTGAGGCCGGTGCT	CACCCTTCAAGTGGGCCCCG	87

References

1. Moghtadaei M, Langille E, Rafferty SA, Bogachev O, Rose RA. Altered heart rate regulation by the autonomic nervous system in mice lacking natriuretic peptide receptor C (NPR-C). *Sci Rep* 2017;**7**:17564.
2. Dorey TW, Moghtadaei M, Rose RA. Altered heart rate variability in angiotensin II-mediated hypertension is associated with impaired autonomic nervous system signaling and intrinsic sinoatrial node dysfunction. *Heart Rhythm* 2020;**17**:1360-1370.
3. Jansen HJ, Mackasey M, Moghtadaei M, Belke DD, Egom EE, Tuomi JM, Rafferty SA, Kirkby AW, Rose RA. Distinct patterns of atrial electrical and structural remodeling in angiotensin II mediated atrial fibrillation. *J Mol Cell Cardiol* 2018;**124**:12-25.
4. Jansen HJ, Mackasey M, Moghtadaei M, Liu Y, Kaur J, Egom EE, Tuomi JM, Rafferty SA, Kirkby AW, Rose RA. NPR-C (Natriuretic Peptide Receptor-C) Modulates the Progression of Angiotensin II-Mediated Atrial Fibrillation and Atrial Remodeling in Mice. *Circ Arrhythm Electrophysiol* 2019;**12**:e006863.
5. Mackasey M, Egom EE, Jansen HJ, Hua R, Moghtadaei M, Liu Y, Kaur J, McRae MD, Bogachev O, Rafferty SA, Ray G, Kirkby AW, Rose RA. Natriuretic Peptide Receptor-C Protects Against Angiotensin II-Mediated Sinoatrial Node Disease in Mice. *JACC Basic Transl Sci* 2018;**3**:824-843.
6. Krishnaswamy PS, Egom EE, Moghtadaei M, Jansen HJ, Azer J, Bogachev O, Mackasey M, Robbins C, Rose RA. Altered parasympathetic nervous system regulation of the sinoatrial node in Akita diabetic mice. *J Mol Cell Cardiol* 2015;**82**:125-135.
7. Azer J, Hua R, Krishnaswamy PS, Rose RA. Effects of natriuretic peptides on electrical conduction in the sinoatrial node and atrial myocardium of the heart. *J Physiol* 2014;**592**:1025-1045.
8. Egom EE, Vella K, Hua R, Jansen HJ, Moghtadaei M, Polina I, Bogachev O, Hurnik R, Mackasey M, Rafferty S, Ray G, Rose RA. Impaired sinoatrial node function and increased susceptibility to atrial fibrillation in mice lacking natriuretic peptide receptor C. *J Physiol* 2015;**593**:1127-1146.
9. Liu J, Dobrzynski H, Yanni J, Boyett MR, Lei M. Organisation of the mouse sinoatrial node: structure and expression of HCN channels. *Cardiovasc Res* 2007;**73**:729-738.
10. Hua R, MacLeod SL, Polina I, Moghtadaei M, Jansen HJ, Bogachev O, O'Blenes SB, Sapp JL, Legare JF, Rose RA. Effects of Wild-Type and Mutant Forms of Atrial Natriuretic Peptide on Atrial Electrophysiology and Arrhythmogenesis. *Circ Arrhythm Electrophysiol* 2015;**8**:1240-1254.
11. Springer J, Azer J, Hua R, Robbins C, Adamczyk A, McBoyle S, Bissell MB, Rose RA. The natriuretic peptides BNP and CNP increase heart rate and electrical conduction by stimulating ionic currents in the sinoatrial node and atrial myocardium following activation of guanylyl cyclase-linked natriuretic peptide receptors. *J Mol Cell Cardiol* 2012;**52**:1122-1134.
12. Cifelli C, Rose RA, Zhang H, Voigtlaender-Bolz J, Bolz SS, Backx PH, Heximer SP. RGS4 regulates parasympathetic signaling and heart rate control in the sinoatrial node. *Circ Res* 2008;**103**:527-535.